Joint spectral retrievals of ozone with Suomi NPP CrIS augmented by S5P/TROPOMI

Edward Malina[1], Kevin W. Bowman[1], Valentin Kantchev[2], Le Kuai[1], Thomas P. Kurosu[1], Kazuyuki Miyazaki[1], Vijay Natraj[1], Gregory B. Osterman[1], Fabiano Oyafuso[1], and Matthew D. Thill[1]

[1]Jet Propulsion Laboratory, California Institute of Technology, Pasadena, California, USA
[2]Swift Software Group, Glendale, California, USA

Correspondence: Edward Malina (edward.malina.13@ucl.ac.uk)

Abstract. The vertical distribution of ozone plays an important role in atmospheric chemistry, climate change, air pollution, and human health. Over the twenty-first century, spaceborne remote sensing methods and instrumentation have evolved to better determine this distribution. We quantify the ability of ozone retrievals to characterise this distribution through a sequential combination of thermal infrared (TIR) and Ultra Violet (UV) spectral radiances, harnessing co-located TIR measurements from the Cross Track Infrared Sounder (CrIS), onboard the Suomi National Polar-orbiting Partnership (NPP), and UV measurements from the TROPospheric Monitoring Instrument (TROPOMI), which is on the Sentinel 5-Precursor (S5P) satellite. Using the MUlti-SpEctra, MUlti-SpEcies, MUlti-SEnsors (MUSES) algorithm, the sequential combination of TIR and UV measurements, which follows retrievals from each instrument separately, moderately improves the ability of satellites to characterise global ozone profiles, over the use of each instrument/band individually. The CrIS retrievals enhanced by TROPOMI radiances in the Huggins band (325-335 nm) show good agreement with independent datasets both in the troposphere and in the stratosphere in spite of calibration issues in the TROPOMI UV. Improved performance is characterised in the stratosphere from CrIS-TROPOMI, firstly through a modest increase in the degrees of freedom of signal (often between 0.1-0.2). Secondly, through comparisons with the Microwave Limb Sounder, where a global month long comparison shows a mean difference $\sim$x10 lower than either CrIS or TROPOMI individually, and R^2 values 3% higher. In the troposphere, CrIS-TROPOMI and CrIS show similar degrees of freedom for signal, with about 2 globally, but higher in the tropics partitioned equally between the lower and upper troposphere. CrIS-TROPOMI validation with ozonesondes show improved performance over CrIS-only, with a difference in the tropospheric column bias of between 30 and 200% depending on the season. Cross-comparisons with satellite instruments and reanalysis datasets show similar performances in terms of correlations and biases. These results demonstrate that CrIS and CrIS/TROPOMI retrievals have the potential to improve global satellite ozone retrievals, especially with future developments. If spectral accuracy is improved in future TROPOMI calibration, the degrees of freedom of signal in the stratosphere could double when using bands 1 and 2 of TROPOMI (270-330 nm), while tropospheric degrees of freedom of signal could increase by 25%.

Copyright statement. © California Institute of Technology, 2022. Government sponsorship acknowledged.

1 Introduction

Characterisation of the ozone vertical distribution is essential to separate its impacts on climate change, global atmospheric chemistry and human health (Szopa et al., 2021; WHO, 2003). Ozone present in the stratosphere (∼90% of the total) is responsible for filtering out harmful UV radiation in the UV-A and B bands (<300 nm). In the stratosphere, ozone is produced by UV radiation destroying O_2 bonds, and liberated oxygen atoms bonding to form ozone, while it is destroyed by photochemical reactions. Ozone in the troposphere (∼10% of the total) is produced by downward transport of stratospheric ozone, and from the interaction of nitrogen oxides (NO_x = NO + NO_2) and non-methane organic carbons (NMOCs) in the presence of sunlight (Szopa et al., 2021). In the troposphere, NOx is typically the limiting precursor in ozone production, since NMOCs are present in high volumes (Szopa et al., 2021). As a large fraction of global NOx emissions are due to anthropogenic sources, ozone pollution is common in metropolitan areas (Jaffe and Wigder, 2012), and has a typical lifetime from several hours to several weeks depending on the local conditions (Young et al., 2013). In the troposphere, ozone acts as a greenhouse gas (GHG), contributing to atmospheric radiative forcing, as well as acting as a pollutant near the surface (Bowman et al., 2013; IPCC, 2013). Therefore, tropospheric ozone variability impacts both human health and climate change and is not well understood. This is underscored by the classification of tropospheric ozone by the National Academy of Sciences 2017 decadal survey as a 'most important' objective (NASES, 2018).

In order to understand ozone variability, the vertical distribution of ozone must be quantified; this can be achieved through a number of remote sensing or in-situ methods. For example, electrochemical concentration cell ozonesondes, which measure ozone concentration via chemical means, are attached as instruments to balloons which measure from the surface up to 30 km altitude (Komhyr et al., 1995). While highly accurate, ozonesondes offer limited coverage, meaning that satellite instruments must be used to identify global ozone variations. There is significant heritage in using satellite instruments to estimate ozone. TIR instruments use the ν_3 spectral region (∼9.6 μm), which is sensitive to variations in pressure and temperature, yielding the most information in the free troposphere. Instruments built to exploit the TIR spectral regions include the Tropospheric Emissions Spectrometer (TES) (Bowman et al., 2006), the Infrared Atmospheric Sounding Interferometer (IASI) (Clerbaux et al., 2010), the Atmospheric Infrared Sounder (AIRS) (Fu et al., 2018), and the Cross-track Infrared Sounder (CrIS) (Bloom, 2001). The CrIS instrument is present on multiple satellites (e.g., Suomi NPP and NOAA-20), and is also expected to be on future satellites (NOAA-21 and 22). UV instruments derive atmospheric profile information about ozone through back-scattered solar UV radiance. The UV measurement is primarily sensitive to the stratosphere due to Rayleigh scattering (Chance et al., 1997); vertical sensitivity is, therefore, limited in the troposphere. Instruments with spectral windows in the UV include the Total Ozone Mapping Spectrometer (TOMS) (Stolarski et al., 1991), the Global Ozone Monitoring Experiment (GOME) (Liu et al., 2006), GOME-2 (Cai et al., 2012), the Ozone Monitoring Instrument (OMI) (Kroon et al., 2011), the SCanning Imaging Absorption SpectroMeter for Atmospheric CHartographY (SCIAMACHY) (Eichmann et al., 2004), the Ozone Mapper Product Suite (OMPS) Nadir Mapper (NM) and Nadir Profiler (NP) (Flynn et al., 2014; Seftor et al., 2014), and the Sentinel-5P (S5P) TROPOspheric Monitoring Instrument (TROPOMI) (Zhao et al., 2021).

These instruments, and many others (e.g., Michelson Interferometer for Passive Atmospheric Sounding (MIPAS) (Fischer et al., 2008)) have yielded a multi-decadal record of ozone variation in the atmosphere. Future planned instruments include (in the TIR) IASI-Next Generation (NG; (Crevoisier et al., 2014)) and Geostationary and Extended Orbits (GeoXO; (NOAA, 2022)). In the UV, Sentinels 4 and 5 (Ingmann et al., 2012), Tropospheric emissions: Monitoring of pollution (TEMPO) (Zoogman et al., 2017) and the Geostationary Environmental Monitoring Spectrometer (GEMS) (Nicks et al., 2018) will augment this record.

All of the above instruments rely on using either TIR or UV wavelengths, thus leaving a gap in the characterisation of the lower troposphere. This is problematic for understanding the impact of ozone in the boundary layer. A proposed solution to this problem is to perform multi-spectral retrievals by combining TIR and UV measurements. In particular, this can be implemented using different instruments from multiple satellites. Multi-spectral satellite retrievals have been shown to improve sensitivity to lower tropospheric ozone (Landgraf and Hasekamp, 2007; Luo et al., 2013; Cuesta et al., 2013, 2018; Fu et al., 2013, 2018; Natraj et al., 2011; Worden et al., 2007b) and also for other trace gases (e.g. methane) (Deeter et al., 2014; Fu et al., 2016; Worden et al., 2015). In addition, there is the opportunity to combine TIR and UV information from future instruments such as IASI-NG and Sentinel 4, and incorporate information from Chemical Reanalysis to further improve knowledge of tropospheric ozone (Colombi et al., 2021). The methods used in this paper will, therefore, be applicable to the next generation of satellite instruments.

The aim of this paper is to build on the previous generation of joint spectral retrievals pioneered by TES and OMI and more recently AIRS and OMI measurements, by characterising and quantifying the performance of ozone profile retrievals using radiance measurements from CrIS and TROPOMI. The utility of joint CrIS-TROPOMI retrievals have been shown previously, initially through simulations (Fu et al., 2018), and more recently using operational data (Mettig et al., 2021, 2022). However, this work utilises different portions of the spectral bands. CrIS and TROPOMI orbit in formation, typically viewing the same scene within 10 minutes, thus offering an excellent opportunity for joint retrievals. For retrievals, we use the MUlti-SpEctra, MUlti-SpEcies, MUlti-SEnsors (MUSES) retrieval algorithm, which is a core part of the TRopospheric Ozone and its Precursors from Earth System Sounding (TROPESS) pipeline (https://tes.jpl.nasa.gov/tropess/get-data/products/). TROPESS, which has considerable heritage from multi-spectral, multi-instrument retrieval algorithms for the UV and the TIR, produces long term, Earth science data records with uncertainties and observation operators (Bowman et al., 2002; Kulawik et al., 2006; Worden et al., 2007b; Natraj et al., 2011; Luo et al., 2013; Fu et al., 2013, 2018; Kulawik et al., 2021).

TROPESS products have been extensively used for scientific analyses; for example, ozone retrievals from CrIS have been assimilated into reanalysis datasets to understand tropospheric ozone during the COVID lock-downs (Miyazaki et al., 2021). Carbon monoxide products from TROPESS/CrIS have been used to understand the impact of wildfires in Australia (Byrne et al., 2021). CrIS-TROPOMI ozone products will join the TROPESS data record for use in scientific analysis.

This paper is structured as follows: The instruments used in this study are identified in Sect. 2. Section 3 details the MUSES algorithm and the characteristics of a subset of ozone retrievals from this algorithm. Section 4 presents some sample results from the joint retrievals, and Sect. 5 shows validation and cross-comparison studies between the MUSES retrieval results, and

Table 1 Characteristics of the Suomi NPP CrIS bands.

Band (Name)	Spectral range (cm^{-1})	Spectral resolution (cm^{-1})	Spatial resolution (diameter km)
Band 1 (Long-Wave)	648.75-1096.25	FSR/NSR:0.625,	14
Band 2 (Mid-Wave)	1208.75-1751.25	FSR:0.625, NSR:1.25	14
Band 3 (Short-Wave)	2153.75-2551.25	FSR:0.625, NSR:2.5	14

retrievals from third party algorithms. Finally, we analyse the results in Sect. 6 and infer conclusions about the performance of MUSES with respect to the multispectral retrievals.

2 Instruments

2.1 Suomi NPP CrIS

CrIS is on the Suomi National Polar-orbiting Partnership (NPP) satellite in a near-polar, sun-synchronous, 828 km altitude orbit with a 13:30 ascending node crossing time and has been operational since October 28, 2011 (Han et al., 2013). Suomi NPP includes several satellite instruments relevant to ozone profile retrievals, including both the OMPS-Nadir Mapper (NM) and Nadir Profiler (NP), and the Visible Infrared Imaging Radiometer Suite (VIIRS). A second copy of CrIS is also aboard NOAA's Joint Polar Satellite System (JPSS) NOAA-20, launched in 2017; the CrIS instrument is also planned to be included on a series of follow-on satellites over the coming decade. However, CrIS on NOAA-20 and 21 will not fly in formation with TROPOMI. While the focus of this paper is the CrIS instrument on the Suomi NPP satellite, the techniques are applicable to the other instruments as well. CrIS is a nadir viewing Fourier Transform Spectrometer (FTS) that measures TIR radiances in the three spectral bands in either Normal Spectral Resolution (NSR) or Full Spectral Resolution (FSR) identified in Table 1. It provides daily global measurements with a swath width of 2300 km, sampled at 30 cross-track positions, with each position consisting of a 3×3 array of pixels with about a 14 km diameter field of view. The wide spectral range and high spatial sampling allows CrIS to retrieve a range of atmospheric composition products, including additional trace gases other than ozone, such as ammonia and carbon monoxide, as well as high resolution temperature and water vapor profiles, useful for numerical weather prediction (Smith and Barnet, 2020).

The extensive time period of data from Suomi NPP CrIS has led to significant work towards generating a long term record of numerous trace gases from the TROPESS product (Fu et al., 2018), and other projects such as the Community Long-term Infrared Microwave Combined Atmospheric Product System (CLIMCAPS) (Smith and Barnet, 2019, 2020), as well as single field of view (FoV) products (Xiong et al., 2022). Note that up until February 2020 Suomi NPP CrIS was providing spectra in both NSR and FSR formats, after which NSR was discontinued. This means a shorter time record is available for joint CrIS-TROPOMI using NSR, therefore this paper focuses on FSR data, which are available from December 2014. However, both CrIS NSR and FSR data is available as a part of the TROPESS project.

Table 2 Characteristics of S5P/TROPOMI bands.

Band (name)	Spectral range (nm)	Spectral resolution (nm)	Spatial resolution (km^2)
Band 1 (UV1)	267-300	0.45-0.5	28x28.8
Band 2 (UV2)	300-332	0.45-0.5	5.6x3.6
Band 3 (UVIS)	305-400	0.45-0.65	5.6x3.6
Band 4 (VIS)	400-499	0.45-0.65	5.6x3.6
Band 5 (NIR1)	661-725	0.34-0.35	5.6x3.6
Band 6 (NIR2)	725-786	0.34-0.35	5.6x3.6
Band 7 (SWIR3a)	2300-2343	0.227	5.6x7.2
Band 8 (SWIR3b)	2343-2389	0.225	5.6x7.2

In May 2021, Suomi NPP CrIS reported failures in the long-wave channels of the 'side 2' electronics suite (NOAA, 2021). In response the instrument was switched to the 'side 1' electronics in order to retain use of the long-wave (band 1) channels (Iturbide-Sanchez et al., 2021). However, the mid-wave (band 2) channels of the side 1 electronics are non-functioning. Since ozone information in the TIR is mostly in the long-wave region, the loss of the mid-wave channels will not impact ozone retrievals to a significant degree. We provide evidence of the impact through an assessment presented in Appendix A, which identifies a minor loss of sensitivity in the retrieved profiles. However, the data presented in this study is from 2020; therefore, this reported issue will not affect any of the presented results.

2.2 S5P/TROPOMI

The Sentinel-5P (S5P) satellite (https://sentinel.esa.int/web/sentinel/missions/sentinel-5p/satellite-description) was launched in October 2017 with the aim of providing global information on air quality and greenhouses gases (GHGs) (Veefkind et al., 2012). S5P is in a mid-afternoon low Earth orbit (13:30 ascending node crossing time) in a tandem orbit with the Suomi NPP satellite. The TROPOMI instrument onboard S5P is an imaging spectrometer with a swath width of roughly 2600 km on the ground, providing data in eight separate wavebands. For each band, the swath width is split up into 'cross track' pixels, which form the individual instrument measurements of size indicated by the spatial resolution in Table 2. The spectral response for each band is characterised by the number of spectral pixels and the instrument line shape function (ILSF).

Bands 1, 2 and 3 (UV1, UV2 and UVIS) are sensitive to ozone, and profile retrievals are possible using windows within these bands, with Mettig et al. (2021) using UV1 & UV2 for profile retrievals and Zhao et al. (2021) using UVIS. UV1 & UV2 are located on the same detector, but are binned differently due to the SNR differences in the bands. UV1 & UV2 suffer from calibration issues (Ludewig et al., 2020; Mettig et al., 2021), requiring significant effort to generate L1b spectra of sufficient quality for ozone retrievals. UVIS is not affected to the same degree (although some soft-calibration is still necessary (Zhao et al., 2021). The primary goal of this paper is to ensure high quality retrievals from a spectral combination of CrIS and TROPOMI, rather than maximising the potential of TROPOMI alone. We therefore use TROPOMI UVIS, which is least

affected by calibration errors. In particular, we use the 325-335 nm window in the Huggins band for total ozone column (TOC) retrievals (Garane et al., 2019). The approach described herein can readily accommodate a larger spectral range as TROPOMI calibration improves.

2.3 Validation and cross-comparison datasets

Datasets used for evaluation are split into three types. Cross-comparisons are made with independent ozone retrievals based upon a co-location of one day, with co-location criteria described in each subsection. Chemical reanalysis datasets, which provide global and consistent ozone, can be constrained by multiple satellite observations including precursor data, (e.g., NOx emissions). These cross-comparisons provide insight into how the retrievals are capturing chemical processes. Their data fields use a more stringent co-location criteria owing to their higher data abundance. We further validate the retrievals with ozonesondes. While ozonesondes are the most accurate (5%) for evaluation, they do not have the same sampling density as the other datasets. In order to get a better statistical sampling, coincidence criteria is looser. The combination of these datasets provides a clearer picture of the CrIS/TROPOMI retrieval performance.

2.3.1 Microwave Limb Sounder (MLS)

MLS is a microwave limb sounder aboard the Aura satellite launched in 2004, on a sun-synchronous orbit similar to S5P and Suomi NPP, with an ascending node crossing time of 13:45 (Waters et al., 2006). The similar orbits of Aura, S5P and Suomi NPP, ensure that the maximum distance between the closest MLS, TROPOMI and CrIS pixels is roughly 1000 km and 1.5 hours. MLS measures emissions using seven radiometers in a spectral range between 118 GHz and 2.5 THz. MLS has a spatial sampling of $\sim$ 6 km across track and $\sim$ 200 km along track, and a vertical resolution ranging from 2.5 to 3.5 km starting in the upper troposphere. The ozone retrievals between 9 and 75 km can be used for scientific analysis. MLS has been validated extensively, (Froidevaux et al., 2008; Livesey et al., 2008), and is therefore a key dataset for cross-comparisons with TROPOMI and CrIS in the stratosphere.

2.3.2 AIRS-OMI

The NASA A-Train satellites are in a near-polar sun-synchronous, $\sim$700 km altitude orbit with an ascending node crossing time of $\sim$13:30 local time. In the A-train is the Aqua satellite, which includes the AIRS instrument. AIRS is a grating spectrometer that measures TIR emissions in the 650–2665 cm^{-1} spectral range, similar to CrIS (Aumann et al., 2003). AIRS is a cross-track scanning grating spectrometer that provides daily global coverage of ozone with a footprint of $\sim$13.5 km. OMI is a nadir-viewing push broom ultraviolet–visible (UV-VIS) grating spectrometer on the AURA satellite that measures solar back-scattered radiance. OMI measures in the 270–500 nm wavelength range (Levelt et al., 2006), covering the same ozone absorption bands as TROPOMI. The ground pixel size of OMI at nadir is $\sim 13 \times 24$ km when using the 310–330 nm spectral range. Since 2009, instrument issues have affected the quality of some OMI pixels limiting the latitudinal range (Levelt et al., 2018).

Ozone profiles from joint AIRS-OMI L1B radiances are retrieved using the MUSES algorithm with spectral windows similar to those employed for the CrIS-TROPOMI product generated here (Fu et al., 2018). The AIRS-OMI retrieval has been extensively validated, and has been used as a key component for chemical re-analysis datasets (Miyazaki et al., 2020b, a).

2.3.3 ~~TROPOMI Offline TOC product~~

~~The operational TROPOMI TOC product is split into two parts, near real time and offline (OFFL). We compare the MUSES TROPOMI TOC retrievals against the OFFL product, which is based on the operational implementation of the GOME-type Direct FITting (GODFIT) v4 algorithm (Garane et al., 2018). GODFIT is designed to retrieve TOC products from satellite nadir-viewing instruments such as SCIAMACHY and GOME/GOME-2. GODFIT simulates radiances in the Huggins band (325–335 nm) and fits to the observed radiances by varying a number of atmosphere parameters, including total ozone and effective scene albedo (Garane et al., 2019). The GODFIT and the MUSES TROPOMI retrieval algorithms aim to quantify similar quantities (identified in detail in Sect.3.3) through the use of similar spectral windows. It is therefore important to benchmark the MUSES TROPOMI algorithm against the GODFIT algorithm. However, GODFIT and the MUSES TROPOMI algorithm have a number of differences including ancillary data and retrieval strategy that will lead to different ozone values. Most notably, GODFIT is a scalar retrieval algorithm, i.e., the TOC is determined by multiplying the a priori ozone profile by a fixed value, while MUSES is a profile fitting algorithm.~~

2.3.3 ~~Chemical reanalysis Cross-Comparisons~~

~~To improve the understanding of emission variability and the processes controlling atmospheric composition, several chemical reanalysis products have been produced by integrating satellite measurements through chemical data assimilation (Sandu and Chai, 2011) . Chemical data assimilation is the process through which atmospheric models incorporate additional information from observations, such as satellite observations, to generate an optimal representation of atmospheric composition. Based on long-term chemical data assimilation, chemical reanalysis is a systematic approach to create a long-term data record consistent with model processes and observations, which mitigates the limitations of current observing systems using models.~~

~~Two independent chemical reanalysis products are used for cross-comparison in this study. First, the Copernicus Atmospheric Monitoring Service (CAMS) reanalysis consists of 3-dimensional time-varying atmospheric composition fields, including ozone. The CAMS reanalysis was produced using data assimilation from the ECMWF Integrated Forecasting System with 60 hybrid sigma/pressure (model) levels in the vertical, interpolated to 25 pressure levels with the top level at 0.1 hPa (Flemming et al., 2017). The CAMS reanalysis infers only the atmospheric state, not emissions.~~

~~The second reanalysis dataset is the Tropospheric Chemistry Reanalysis Version 2 (TCR-2) obtained from the JPL Multi-mOdel Multi-cOnstituent Chemical data assimilation (MOMO-Chem) system, which uses an ensemble Kalman filter (EnKF) data assimilation technique (Miyazaki et al., 2020a, b) to simultaneously estimate concentrations and emissions of various species. For the years 2005–2020 at 1.1° horizontal resolution assimilation is performed for ozone, CO, NO_2, HNO_3, and SO_2 using OMI, SCIAMACHY, GOME-2, TES, MLS, and MOPITT satellite measurements. The evaluation results demonstrate the capability of the chemical reanalysis to improve understanding of the processes controlling variations in atmospheric~~

~~composition, including long-term changes in near-surface air quality and emissions (Miyazaki et al., 2021). For the 2020 year comparisons used in this study, the tropospheric ozone in MOMO-Chem was constrained by measurements of precursors (OMI NO_2 and MOPITT CO) and stratospheric concentrations (MLS ozone and HNO_3), whereas no tropospheric ozone data was assimilated facilitating independent validation of the satellite tropospheric ozone products.~~

2.3.3 Ozonesondes

Ozonesondes are sensors that use a dilute solution of potassium iodide to produce a weak electrical current proportional to the ozone concentration of the sampled air (Komhyr et al., 1995). These sensors are placed on balloons and provide in-situ data from the surface to the stratosphere (about 35 km) with vertical resolution of 150m and accuracy of 5% (Witte et al., 2017, 2018). The World Ozone and Ultraviolet radiation Data Centre (WOUDC) operates and freely publishes data from these ozonesondes, producing multi-year datasets over global locations. These data are key in the validation of ozone profiles measured by satellite instruments (Thompson et al., 2017), and have previously been used to validate TROPESS ozone products (Worden et al., 2007b; Fu et al., 2018).

3 TROPESS/MUSES

3.1 MUSES CrIS-TROPOMI Retrievals

The joint CrIS-TROPOMI retrieval integrate the CrIS and TROPOMI retrievals identified in Fig. 1 and described in detail in sects. 3.2, 3.3. The MUSES algorithm is described in more detail in sect. 3.4.

The first step in the joint CrIS-TROPOMI retrieval is pairing of the footprints. Our pairing method is as follows:

- Use only daytime CrIS soundings (SZA < 90°).
- Find all CrIS and TROPOMI (UVIS) pixels within a 20 minute time frame (where Suomi-NPP and S5P pass the same scene within ∼10 mins), allowing for some variation in scene overpass times.
- From the current sounding subset, check all pairs that are within < 50 km distance, and select the pair that has the minimum distance.

As identified in Table 2, the TROPOMI bands have varying spatial resolution; therefore, for any future work, each band must be paired separately with the same CrIS footprint. Following the pairing, the CrIS-TROPOMI pipeline retrieval is performed as shown in Fig. 1. In summary, all CrIS retrieval steps are performed initially, beginning with improvements of ancillary information such as surface temperature and cloud parameters. For handling clouds in CrIS retrievals, the MUSES algorithm picks each FoV from the 3×3 FoV structure of the CrIS Field of Regard (FoR). Relevant cloud properties (e.g., cloud top height and extinction) for the FoVs are retrieved and passed into the ozone retrieval for quality control, with too optically thick clouds being flagged as poor quality. In contrast, other CrIS ozone algorithms (e.g., CLIMCAPS) use cloud clearing by aggregating cloud-free spectral channels across the 3×3 FoV structure (Susskind et al., 2003), meaning the MUSES CrIS retrieval has x9

higher spatial resolution. Ancillary information is provided by Operational Support Products (OSPs) which include a priori information, covariances, ILSFs. Following the refinement of ancillary information, trace gas retrievals are undertaken, such as water vapour and methane. Information about water vapour, temperature, emissivity and cloud parameters are then passed onto the CrIS ozone retrieval (Table 4). After the CrIS ozone retrieval several other trace gases are retrieved (e.g. CO), but these do not affect the ozone retrieval. The next step is the TROPOMI ozone, which consists of two parts. Initially the cloud fraction is determined from the radiance spectra, followed by the ozone retrieval (Table 6). The initial guess for the TROPOMI ozone profile can be either the a priori vector, or the CrIS retrieval. The next stage is the CrIS-TROPOMI retrieval which is the final retrieval step, where the initial guess can either be the ozone a priori, or the output from the TROPOMI retrieval. Following the retrievals, VMRs are obtained for each retrieval step (i.e., ozone for CrIS, TROPOMI, CrIS-TROPOMI, and the other trace gases from CrIS). Retrieval errors are calculated at each step, and propagated through the retrieval chain, such that the final CrIS-TROPOMI retrieval will incorporate errors from all of the previous steps. The VMRs and errors finally are passed through quality control, after which the final trace gas products are generated. The state vector for the CrIS-TROPOMI retrieval is a combination of the elements identified in Tables 4 and 6, and the spectral windows are a combination of those indicated in Tables 3 and 5.

3.2 CrIS retrieval configuration

The retrieval strategy for CrIS ozone retrievals is shown in Fig 1. The strategy consists of steps to refine atmospheric parameters prior to the retrieval of the ozone (Kulawik et al., 2006; Eldering et al., 2008; Worden et al., 2012). Note that Fig 1 shows CrIS and TROPOMI ozone retrievals feeding into the CrIS-TROPOMI retrieval, these steps are not necessary for the CrIS-TROPOMI retrieval, but may be used to provide an updated ozone initial guess depending on user needs.

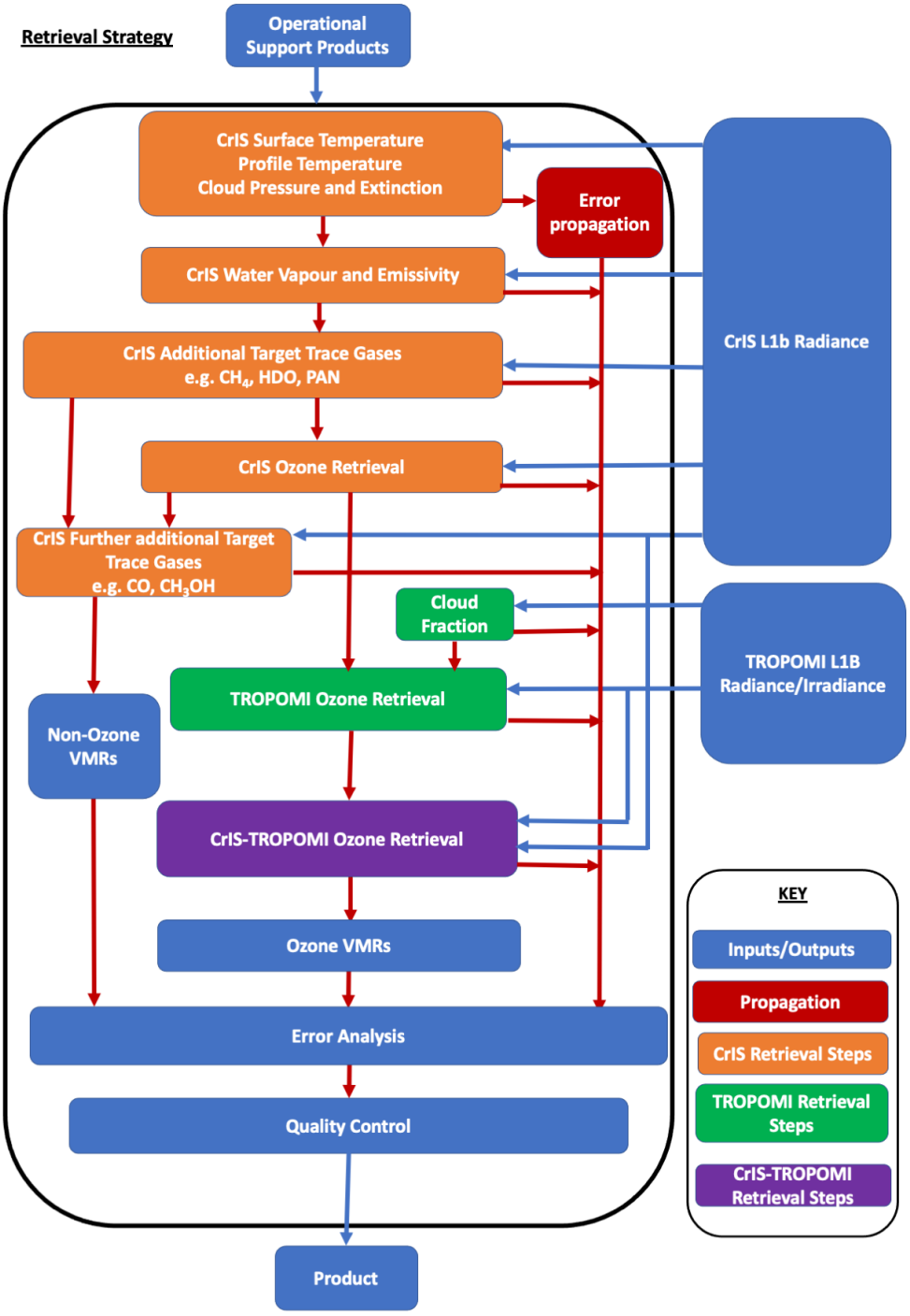

Figure 1. MUSES ozone retrieval pipeline outline for CrIS-TROPOMI. The retrieval steps unique to CrIS and TROPOMI are indicated by the box colours. All steps are used in the CrIS-TROPOMI retrieval, with ozone retrievals and errors calculated in the CrIS and TROPOMI-only steps fed into the CrIS-TROPOMI retrieval. This feed-forward can be enabled or disabled depending on the requirements of the user. The spectral windows and interfering elements for CrIS are described in Table 3 and TROPOMI in Table 5.

The simulated radiance and Jacobians for the MUSES CrIS retrievals are calculated by the fast Optimal Spectral Sampling (OSS) RTM (Moncet et al., 2008, 2015) over a series of micro-windows defined in Table 3. To calculate the synthetic radiances, the OSS RTM is provided the viewing geometry and instrument response function from Version 2 of the CrIS L1b data (Revercomb and Strow, 2018). The RTM also requires the current atmospheric state, $\mathbf{x}$, along with the list of fitting parameters, a priori values and the a priori covariance as identified in Table 4, as well as ancillary data, $\mathbf{b}$ necessary for the simulation but not actively retrieved. The sources of the a priori data (indicated in Table 4) are described in other papers relating to MUSES (Kulawik et al., 2006; Fu et al., 2013, 2018; Worden et al., 2019; Kulawik et al., 2021), but are summarised here: the Model for OZone and Related chemical Tracers (MOZART)-3 and 4 (Brasseur et al., 1998; Park et al., 2004; Emmons et al., 2010) for the ozone profile and covariance. Water vapour, temperature profile and surface temperature data from the Goddard Earth Observing System Model, Version 5 (GEOS-5) (Suarez et al., 2008) and covariance from the National Center for Environmental Prediction (NCEP) reanalysis (Kalnay et al., 1996). The emissivity a priori are taken from the University of Wisconsin-Madison (UOW-M) Global infrared land surface emissivity database (Seemann et al., 2008). The a priori cloud properties come from an 'initial guess' refinement step using brightness temperature differences. The spectroscopic parameters for the target gases and interfering gases are derived from the High Resolution TRANSmission (HITRAN) 2012 database (Rothman et al., 2013).

Table 3 MUSES micro-windows used for CrIS pipeline ozone retrievals. Version 2.0 of the CrIS L1B data product, available on the NASA GES DISC (Revercomb and Strow, 2018), are used in this study.

CrIS Band	**Target**	**Window Start** $[cm^{-1}]$	**Window Stop** $[cm^{-1}]$	**Species**
Long-Wave	O3	950.00	1031.25	H2O, HDO, NH3, O3, CO2
Long-Wave	O3	1043.125	1048.75	H2O, HDO, NH3, O3, CO2
Long-Wave	O3	1068.75	1088.75	H2O, HDO, NH3, O3, CO2, CH4, CFC11, CFC12
Long-Wave	O3	1094.375	1095.00	H2O, CH3OH, HDO, NH3, O3, CO2, CH4, CFC11, CFC12
Mid-Wave	O3	1211.25	1215.00	H2O, HDO, O3, CO2, CH4, N2O
Mid-Wave	O3	1223.75	1227.50	H2O, HDO, O3, CO2, CH4, N2O
Mid-Wave	O3	1258.75	1261.25	H2O, HDO, O3, CO2, CH4, N2O
Mid-Wave	O3	1265.00	1267.50	H2O, HDO, O3, CO2, CH4, N2O
Mid-Wave	O3	1268.75	1271.25	H2O, HDO, O3, CO2, CH4, N2O
Mid-Wave	O3	1311.25	1317.50	H2O, HDO, O3, CO2, CH4, N2O

Table 4 List of parameters in the MUSES/CrIS ozone retrieval state vector, including sources of a priori and covariance

Fitting parameter	Number of parameters	A priori	A priori error
O_3 at each pressure level	25	MOZART-4	MOZART-3 ∼10-40%
H_2O at each pressure level	16	GEOS-5	NCEP ∼ 30%
Surface temperature	1	GEOS-5	0.5 K
Surface emissivity	19	UOW-M database	0.006
Cloud extinction	10	Initial Brightness Temperature Difference	300%
Cloud top pressure	1	500 mbar	100%

3.3 TROPOMI retrieval strategy

For the purposes of joint CrIS-TROPOMI retrievals, we use the Huggins band in UVIS. The retrieval pipeline for TROPOMI is identified by the green boxes in Fig 1, beginning with a cloud fraction guess, followed by the full retrieval. If the cloud fraction is determined to be >0.3, then the retrieval is flagged as poor quality and not considered in further analysis.

The simulated radiance and Jacobians for the MUSES TROPOMI retrievals are calculated by the Vector LInearized Discrete Ordinate Radiative Transfer (VLIDORT) RTM (Spurr, 2006; Spurr et al., 2008). Synthetic radiances are generated by providing VLIDORT viewing geometry and instrument response information from version 1 of the TROPOMI L1b data. All radiances are normalised in the retrieval process using version 1 TROPOMI L1b irradiance products (i.e., $I_{earthshine}/I_{sunshine}$, where I refers to irradiance). The TROPOMI retrieval state vector, along with the a priori source and covariance, is described in Table 6. The ozone profile (and non-retrieved elements such as temperature profiles) are the same as those identified for the CrIS state vector. Additional databases providing further information are as follows: the cloud fraction is determined from the 346.5-347.5 nm window; however, an initial guess is taken from the TROPOMI level 2 cloud product (Loyola et al., 2018). The a priori for the zero-order albedo term is taken from OMI climatology (Kleipool et al., 2008), with the first and second order albedo terms added to allow for non-linear variation of albedo across the spectral band. Thus the effective albedo forms the quadratic equation,

$$A(\lambda) = A_0 + A_1(1 - \lambda/\lambda_0) + A_2(1 - \lambda/\lambda_0)^2, \quad (1)$$

where A is the effective surface albedo at wavelength λ, A_0, A_1 and A_2 are the zero, first and second order parameters fit by MUSES, and λ_0 is the first wavelength.

Digital elevation data are provided by GMTED2010 (Danielson and Gesch, 2011). Serdyuchenko ozone cross sections, as used by the TROPOMI TOC product, are used in the calculation of the ozone optical depth (Serdyuchenko et al., 2014).

Table 5 MUSES micro-windows used for TROPOMI pipeline ozone retrievals. Version 1.0 of the TROPOMI L1B data product, available on the NASA GES DISC, are used in this study

TROPOMI Band	Target	Window Start [nm]	Window Stop [nm]	Species
UVIS	O3	325	335	O3
UVIS	Cloud Fraction	346.5	347.5	Cloud Fraction

Table 6 List of parameters in the MUSES/TROPOMI ozone retrieval state vector, including source of a priori and covariance

Fitting parameter	Number of parameters	A priori	A priori error
O_3 at each pressure level	25	MOZART-4	MOZART-3 $\sim$10-40%
Cloud Fraction	1	Derived from 346.5-347.5 nm	0.05
Ring Scaling	1	1.9	1.0
Irradiance shift	1	0.0	0.02 nm
Radiance/Irradiance shift	1	0.0	0.02 nm
Albedo (zero order)	1	OMI climatology	0.05
Albedo (first order)	1	0	0.05
Albedo (second order)	1	0	0.01

3.4 Algorithm description

The MUSES algorithm is described in detail in other publications (Worden et al., 2007b; Fu et al., 2013; Luo et al., 2013; Fu et al., 2016, 2018), but is summarised here. MUSES is designed to be flexible such that multiple trace gas retrievals from various instrument types are possible. This algorithm has a flexible and generic Radiative Transfer Model (RTM) that covers the entire wavelength range from the UV to the TIR and a nonlinear retrieval algorithm based on the Optimal Estimation (OE) method (Rodgers, 2000). MUSES has a long heritage in retrieving atmospheric parameters from a number of different satellite missions and instruments, including AIRS, TES and OMI, as well as for performing joint spectral retrievals (Bowman et al., 2006; Kulawik et al., 2006; Fu et al., 2013; Luo et al., 2013; Fu et al., 2018; Worden et al., 2019; Kulawik et al., 2021).

MUSES optimally fits the simulated spectral radiance output from a RTM to observed spectral radiance measurements from satellite instruments in order to infer surface and atmospheric parameters. The OE algorithm at the heart of MUSES computes the best-estimate state vector $\hat{\mathbf{x}}$, which represents that atmospheric state and ancillary variables, by minimising the following cost function adapted for multiple instruments:

$$J(\mathbf{x}) = \underbrace{\left[\left[\mathbf{y}_{\mathrm{Cr}} - \mathbf{F}(\mathbf{x}, \mathbf{b}_{\mathrm{Cr}})\right]^T \mathbf{S}_{\epsilon-\mathrm{Cr}}^{-1} \left[\mathbf{y}_{\mathrm{Cr}} - \mathbf{F}(\mathbf{x}, \mathbf{b}_{\mathrm{Cr}})\right]\right]}_{\mathrm{CrIS}}$$

$$+ \underbrace{\left[\left[\mathbf{y}_{\mathrm{TO}} - \mathbf{F}(\mathbf{x}, \mathbf{b}_{\mathrm{TO}})\right]^T \mathbf{S}_{\epsilon-\mathrm{TO}}^{-1} \left[\mathbf{y}_{\mathrm{TO}} - \mathbf{F}(\mathbf{x}, \mathbf{b}_{\mathrm{TO}})\right]\right]}_{\mathrm{TROPOMI}}$$

$$+ (\mathbf{x} - \mathbf{x}_a)^T \mathbf{S}_a^{-1} (\mathbf{x} - \mathbf{x}_a), \quad (2)$$

Cr refers to CrIS and TO refers to TROPOMI. The difference between the observed radiance $\mathbf{y}$ and the simulated radiance $\mathbf{F}(\mathbf{x}, \mathbf{b})$ inversely weighted by the instrument error co-variance matrix $\mathbf{S}_\epsilon$ is represented by the first half of the equation. $\mathbf{F}(\bullet)$ represents the forward model, with $\mathbf{b}$ representing a vector of elements necessary for radiance simulation, but not actively retrieved. The instrument noise $\mathbf{S}_\epsilon$ is obtained from CrIS or TROPOMI L1b files. The difference between the retrieval vector $\mathbf{x}$ and the a priori state $\mathbf{x}_a$ inversely weighted by the a priori covariance matrix $\mathbf{S}_a$ is represented by the second term in Equation 2. Equation 2 is minimised through an iterative update of the state vector based upon the trust-region Levenberg–Marquardt scheme (Bowman et al., 2006):

$$\mathbf{x}_{i+1} = \mathbf{x}_i + \left(\underbrace{\mathbf{K}_{\mathrm{Cr}}^T \mathbf{S}_{\epsilon-\mathrm{Cr}}^{-1} \mathbf{K}_{\mathrm{Cr}}}_{\mathrm{CrIS}} + \underbrace{\mathbf{K}_{TO}^T \mathbf{S}_{\epsilon-TO}^{-1} \mathbf{K}_{TO}}_{\mathrm{TROPOMI}} + \mathbf{S}_a^{-1} + \lambda_i \mathbf{D}^2 \right)^{-1}$$

$$\times \left(\underbrace{\mathbf{K}_{\mathrm{Cr}i}^T \mathbf{S}_{\epsilon-\mathrm{Cr}}^{-1} [\mathbf{y}_{\mathrm{Cr}} - \mathbf{F}(\mathbf{x}_{\mathrm{Cr}i}, \mathbf{b}_{\mathrm{Cr}})]}_{\mathrm{CrIS}} + \underbrace{\mathbf{K}_{\mathrm{TO}i}^T \mathbf{S}_{\epsilon-\mathrm{TO}}^{-1} [\mathbf{y}_{\mathrm{TO}} - \mathbf{F}(\mathbf{x}_{\mathrm{TO}i}, \mathbf{b}_{\mathrm{TO}})]}_{\mathrm{TROPOMI}} \right)$$

$$+ \mathbf{S}^{-1}{}_{\mathrm{a}} (\mathbf{x}_i - \mathbf{x}_a), \quad (3)$$

where λ is the Levenberg-Marquardt parameter, chosen at each iteration step, multiplied by scaling matrix $\mathbf{D}$, the calculation of these values are described in Sects. 5.5 and 6.3 of Moré (1978). The $\lambda\mathbf{D}$ factor is important in controlling the convergence of the algorithm, with small λ values prioritising the speed of the convergence, similar to the Gauss-Newton method, while large values reduce the speed of the convergence, and is similar to the conjugate gradient method. $\mathbf{K}$ represents the Jacobian matrix for the sensitivity of the radiances to the atmospheric state and is defined as $\mathbf{K} = \delta\mathbf{F}(\mathbf{x}, \mathbf{b})/\delta\mathbf{x}$. Eqs. 2 and 3 refer to the joint CrIS-TROPOMI retrieval, and therefore are a combination of the elements in Tables 4 and 6. For the CrIS-only and TROPOMI-only retrievals shown in Fig. 1, Eqs. 2 and 3 are modified to take into account only the relevant instruments.

3.5 TROPOMI, CrIS and CrIS-TROPOMI Characterisation

The following analysis compares ozone retrievals in sub-columns and individual pressure levels. The sub-columns are defined as the troposphere (surface to the tropopause), lower troposphere (surface to 500 hPa), upper troposphere (500 hPa to the tropopause) and the stratosphere (tropopause to 1 hPa).

3.5.1 Quality of fit

The spectral windows used in the joint CrIS-TROPOMI window shown in Fig. 2. For TROPOMI, the whole spectral range is relevant to the ozone retrieval, from UV1 through to part of UVIS (UVIS extends to 400 nm, but ozone absorption is not significant beyond 340 nm). However, these are not fully exploited because of calibration errors.

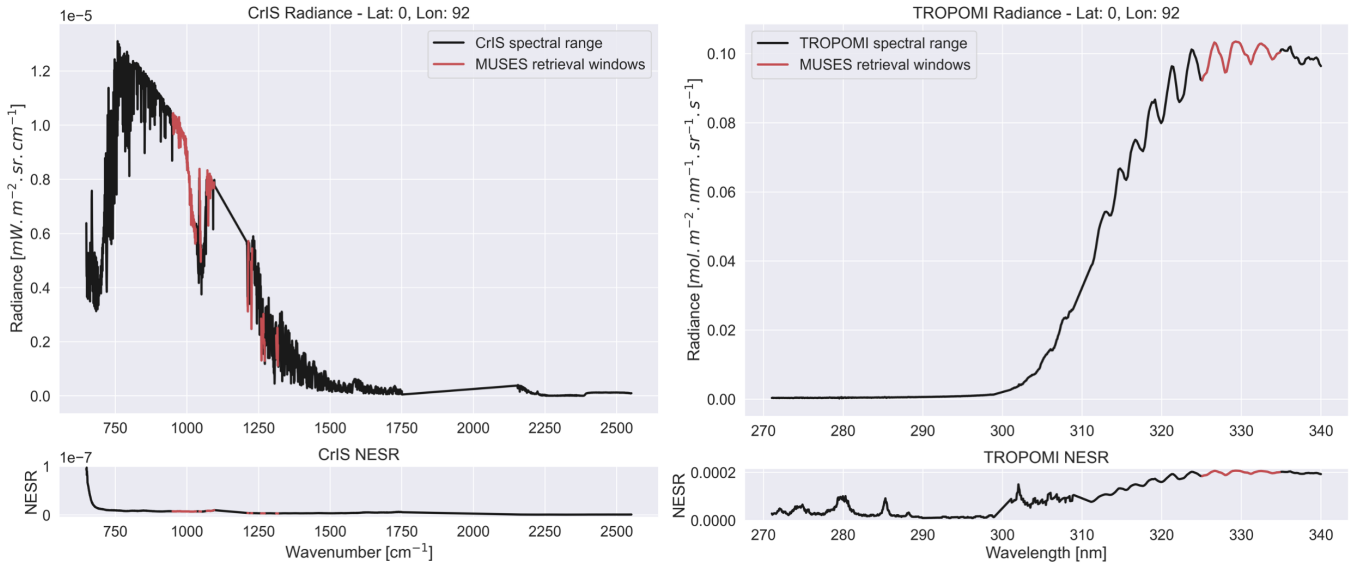

Figure 2. Example radiance from CrIS (left hand plot) and TROPOMI (right hand plot). The bold black line in the top plots indicates the radiance from a specific case over the indicated lat/lon. The red areas indicate the retrieval ~~windows~~ fits used in this study. The bottom plot indicates the Noise Equivalent Spectral Radiance (NESR) as defined in Zavyalov et al. (2013), for this specific retrieval case.

The quality of the fit in these windows is expressed through multiple metrics, two of which are highlighted here. First, we have the normalised residual radiance Root Mean Squared Error (RMSE), which is the RMSE between observed and calculated radiance normalised by measurement error, indicating the impact of any large localised deviations. Second, we use the normalised absolute residual radiance mean, which identifies the mean bias between the calculated and measured spectra, again normalised by the measurement error. Table 7 identifies examples of these metrics for the CrIS-TROPOMI, TROPOMI and CrIS cases, as well as the standard deviation over 10k cases on a day in August 2020.

Table 7 Example CrIS, TROPOMI and CrIS-TROPOMI fit quality statistics based on 10k retrievals. All statistics are normalised by measurement error)

Statistic (Normalised)	**Mean**	**Standard Deviation**
CrIS Residual radiance RMSE	1.04	0.34
CrIS Absolute residual radiance mean	-0.002	0.0340
TROPOMI Residual radiance RMSE	1.17	0.171
TROPOMI Absolute residual radiance mean	0.07	0.08
CrIS-TROPOMI Residual radiance RMSE	1.42	0.373
CrIS-TROPOMI Absolute residual radiance mean	0.055	0.019

The results shown in Table 7 suggest that TROPOMI retrievals have a larger absolute mean residual radiance, which is more variable over the whole dataset, than either CrIS or CrIS-TROPOMI retrievals. The RMSE values indicate larger standard deviations in the CrIS-TROPOMI and CrIS cases, while CrIS has the lowest mean RMSE. This suggests more variability in the CrIS fits which is understandable given the wider retrieval windows, while TROPOMI has a more constant bias. These quality of fit parameters form a part of the MUSES quality assurance procedure (described in 3.6).

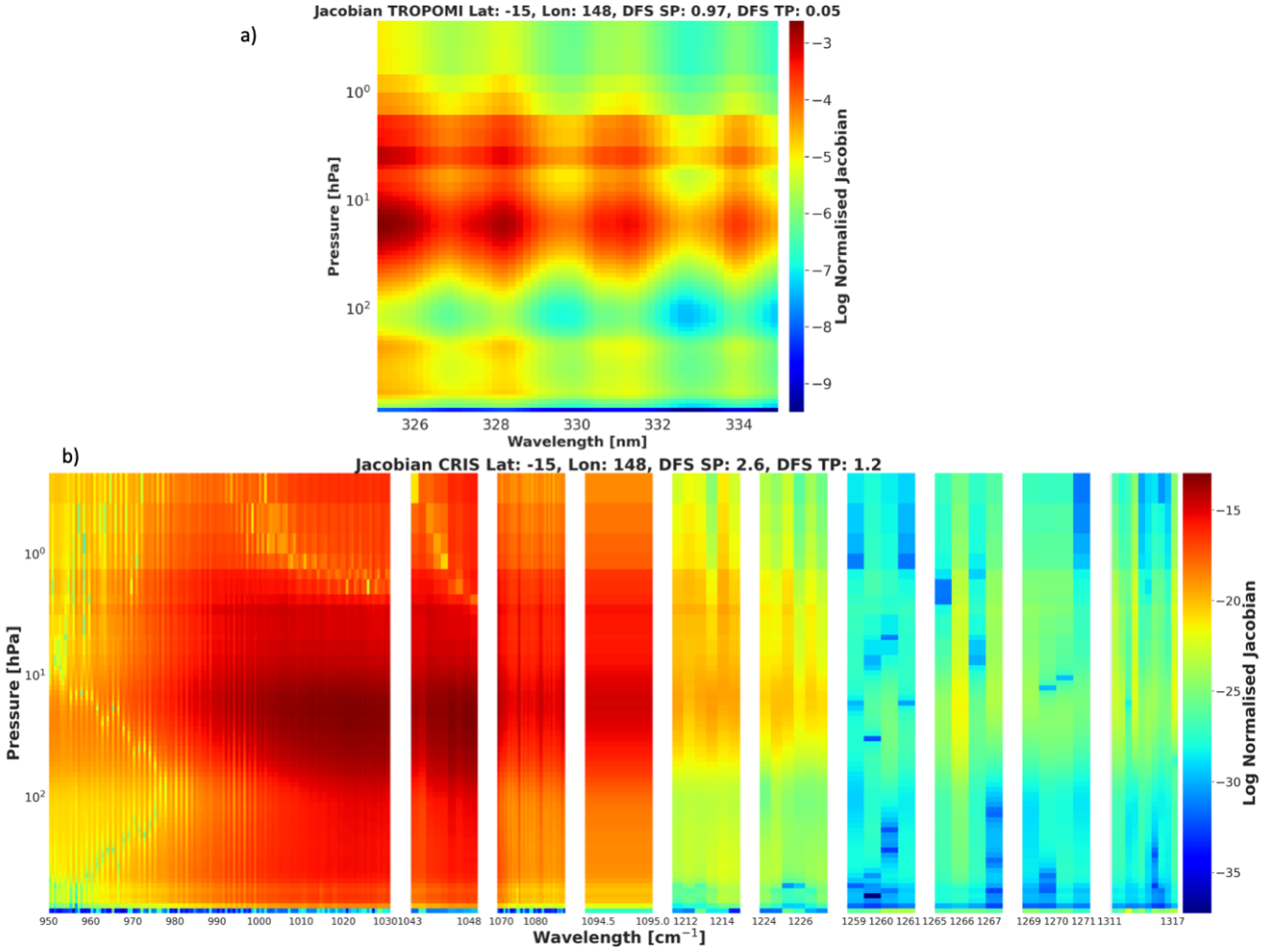

Figure 3. Example normalised Jacobians on a logarithmic scale from TROPOMI (a) and CrIS (b). Jacobians are indicated for all MUSES pressure levels, normalised for each instrument. The square root of the diagonal elements of the measurement error matrix is used as the normalising element. Jacobians for the CrIS retrieval are split into separate panels, identifying the Jacobians for each spectral window (Table 3). The latitude and longitudes are indicated in the title of each panel, as well the Degrees of Freedom of Signal (DFS) values for the stratospheric (SP) and tropospheric profiles (TP).

.

The TROPOMI ozone Jacobians indicated in Fig. 3 a) show greater sensitivity in the UV to stratospheric ozone. Sensitivity decreases significantly with increasing wavelength and decreasing altitude. For the CrIS Jacobians shown in Fig. 3 b) ~~there is more ozone sensitivity in the lower stratosphere. In general, (TIR) have greater sensitivity in the lower troposphere (surface to ~500 hPa) whereas the UV is more sensitive to upper tropospheric (~500 hPa to tropopause) ozone. For the CrIS Jacobians, the majority of ozone sensitivity is~~ peak ozone sensitivity is found in the 9.6 ~~micron band~~ and 10.43 micron bands primarily

between 100 and 10 hPa, but does extend through to the lower troposphere (1000 hPa) and the upper stratosphere (1 hPa), indicating sensitivity through the whole atmosphere, as opposed to TROPOMI-only. It is important to note that the Jacobians identified in Fig. 3 are for a single retrieval in the tropics, where the tropospheric profile DFS are significant (1.2). Other examples (in high latitudes) not highlighted in this paper show less sensitivity in the lower troposphere in the 950-1030 cm^{-1} window. The ability of CrIS-TROPOMI and CrIS to resolve information in the lower troposphere is further highlighted by the DFS presented in Fig. 5.

3.5.2 Information content

For moderately non-linear problems, the OE method allows for the characterisation of the relationship between the truth and the retrieved state vector as follows Rodgers (2000)

$$\hat{\mathbf{x}} = \mathbf{x}_a + \mathbf{A}[\mathbf{x}_{true} - \mathbf{x}_a] + \mathbf{G}\epsilon, \tag{4}$$

where $\mathbf{A}$ is the Averaging Kernel (AK), which indicates the sensitivity of the retrieved solution to the 'truth', i.e. the sensitivity of the retrievals to changes in trace gas concentration in the atmosphere. $\mathbf{x}_{true}$ is the true state vector, $\mathbf{G}$ is the Gain matrix Eq 5:

$$\mathbf{G} = \left(\mathbf{K}_{Cr}^T \mathbf{S}_{\epsilon-Cr}^{-1} \mathbf{K}_{Cr} + \mathbf{K}_{TO}^T \mathbf{S}_{\epsilon-TO}^{-1} \mathbf{K}_{TO} + \mathbf{S}_a^{-1}\right)^{-1} \times \left[\mathbf{K}_{Cr}^T \mathbf{S}_{\epsilon-Cr}^{-1} + \mathbf{K}_{TO}^T \mathbf{S}_{\epsilon-TO}^{-1}\right], \tag{5}$$

ϵ is the spectral noise of the satellite instrument. The use of the OE method in MUSES allows for the generation of the AK and error matrices for each retrieval, which are defined as

$$\mathbf{A} = \mathbf{G}\mathbf{K} = \frac{\partial \hat{\mathbf{x}}}{\partial \mathbf{x}_{true}}, \tag{6}$$

and the total covariance error

$$\mathbf{S} = \underbrace{(\mathbf{I} - \mathbf{A})\mathbf{S}_a(\mathbf{I} - \mathbf{A}^T)}_{smoothing\ error} + \underbrace{\mathbf{G}\mathbf{S}_\epsilon\mathbf{G}^T}_{measurement\ error}, \tag{7}$$

from the AK, we can determine the number of independent pieces of information in the retrieval, known as the degrees of freedom for signal (DFS), defined as DFS = trace($\mathbf{A}$). DFS values larger than 1 indicate the capability to determine some profile information. We define DFS values in discrete portions of the atmosphere. The tropospheric profile covers from the surface pressure to the tropopause (as defined by GEOS-5). The lower tropospheric profile is from the surface pressure to 500 hPa and the upper tropospheric profile is from 500 hPa to the tropopause. The stratospheric profile is from the tropopause to the top of the atmosphere.

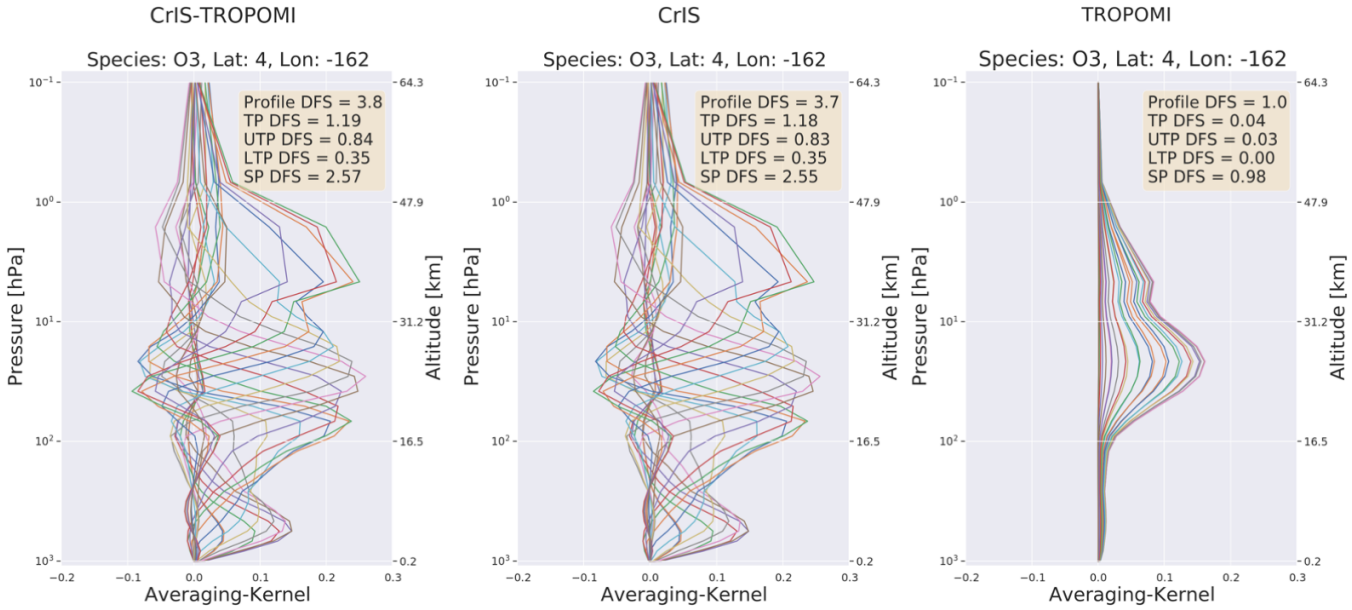

Figure 4. Example AKs from MUSES retrievals in August 2020. The left hand plot indicates the AKs for CrIS-TROPOMI, the middle for CrIS and the right-hand plot for TROPOMI. The DFS values for these AKs are indicated in the labels for each plot. Profile DFS shows the DFS for the whole retrieved profile, TP for the tropospheric profile, UTP for the upper tropospheric profile, LTP for the lower tropospheric profile and SP for the stratrospheric profile. The different colours represent the AK for each pressure level.

In Fig. 4 examples of AKs for each instrument on August 12 are shown. The TROPOMI AK (right panel) indicates 1 DFS for the whole profile as expected from the Huggins band, with almost all of the information confined to the stratosphere. The CrIS AK indicates 1 DFS in the troposphere and 2.5 in the stratosphere, with the total profile generating about 3.6 DFS. Referring to Fig. 5, at similar latitudes total DFS values can be up to 4.5, indicating the shown example is a relative outlier. For comparison purposes Zhao et al. (2021) indicates 1.5-2 DFS over the whole profile for TROPOMI UVIS, and Mettig et al. (2021) calculate 6.5 for the whole profile in UV1 & UV2, with 1.5 for the troposphere. The implication is that TROPOMI and CrIS have similar performance in the troposphere for UV1 & UV2. This comparable performance can change however, given the performance of CrIS is dependent on thermal contrast. The joint profile qualitatively retains the characteristics of the CrIS AK, while quantitatively, we note minor increases in the profile, stratospheric and tropospheric DFS values in this case, while others show more variation, as can be seen in Fig. 5. In comparison, Mettig et al. (2022) show a CrIS-TROPOMI retrieval based on UV1 & UV2 of TROPOMI; the joint retrieval AK is dominated by TROPOMI in this case with the CrIS retrieval adding about 1 DFS to the TROPOMI AK for the case shown.

Comparisons of the AKs in Fig. 4 with the Jacobians in Fig. 3 provide some explanation for the indicated sensitivities. For TROPOMI, the Jacobians indicate sensitivity for all wavelengths only at a small number of pressure levels in the stratosphere. Therefore, the AK peaks at one location in the stratosphere. CrIS Jacobians, in contrast, show sensitivity at multiple pressure

levels ~~due to the many spectral windows used for the CrIS retrieval~~through the troposphere and stratosphere. This is indicated by the multiple peaks in the AKs.

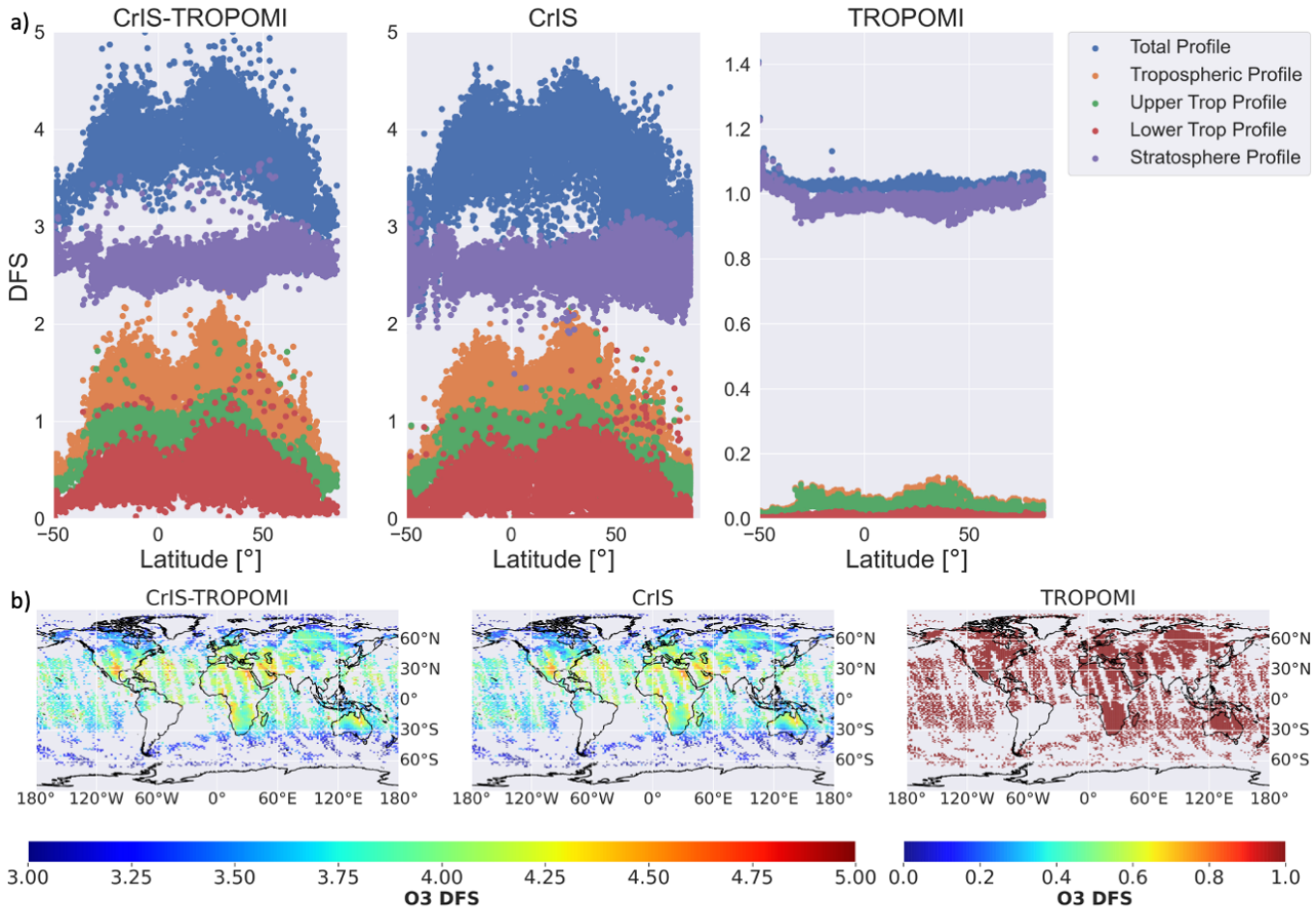

Figure 5. (a) DFS by latitude over the globe on a day in August 2020 for each of the instruments under investigation in this study, as indicated in the subplot titles. DFS are identified for the whole retrieval profile, as well as sub-columns as shown in the legend. In this figure, the upper troposphere refers to the region from 500 hPa to the tropopause, and lower troposphere is the region from the surface to 500 hPa. (b) Spread of profile DFS over the globe for a day in August 2020, with the order of subplots the same as those in (a). Two colour bars are shown, due to the large differences in DFS between CrIS-TROPOMI/CrIS and TROPOMI.

The global spread of DFS values is investigated in Fig. 5. The latitudinal spread of DFS values shown in row a) of Fig. 5 generally indicates similar DFS values for each sub-column for CrIS and CrIS-TROPOMI, as predicted by Fig 4. For both CrIS and CrIS-TROPOMI, we note that the profile and tropospheric column DFS values tend to be at a maximum in the region surrounding the equator, while the DFS values in the stratosphere remain largely consistent over all latitudes. For TROPOMI, as suggested by Fig 4, DFS values are small in the troposphere over all latitudes, while those in the whole profile/stratosphere

remain largely constant over the globe. Considering the global spread of profile DFS values for each instrument, as shown by row b) of Fig. 5, CrIS and CrIS-TROPOMI have similar patterns, with the region surrounding the equator showing the largest values.

Note that according to the histograms in Fig. B1 b) and c) CrIS-TROPOMI ~~generally shows~~ can exhibit higher DFS values than CrIS alone in ~~both the troposphere and the~~ the stratosphere, although as indicated by Fig. 4, the differences can be subtle. The differences are very minor for the troposphere, so this is not obvious from the histograms. For example, focusing on the Atlantic Ocean, there are regions with clearly improved DFS values from CrIS-TROPOMI, as opposed to CrIS. Further, there are ~~numerous~~ a small number of cases for CrIS and CrIS-TROPOMI where DFS values of ~~~~more than 2 are achieved in the whole troposphere (Fig. B1). This suggests that CrIS-TROPOMI and CrIS are highly useful for tropospheric ozone estimation. For the TROPOMI retrievals, a constant DFS value of roughly 1 is apparent all over the globe, indicating that local conditions have limited impact on the TROPOMI retrieval.

3.5.3 Uncertainties

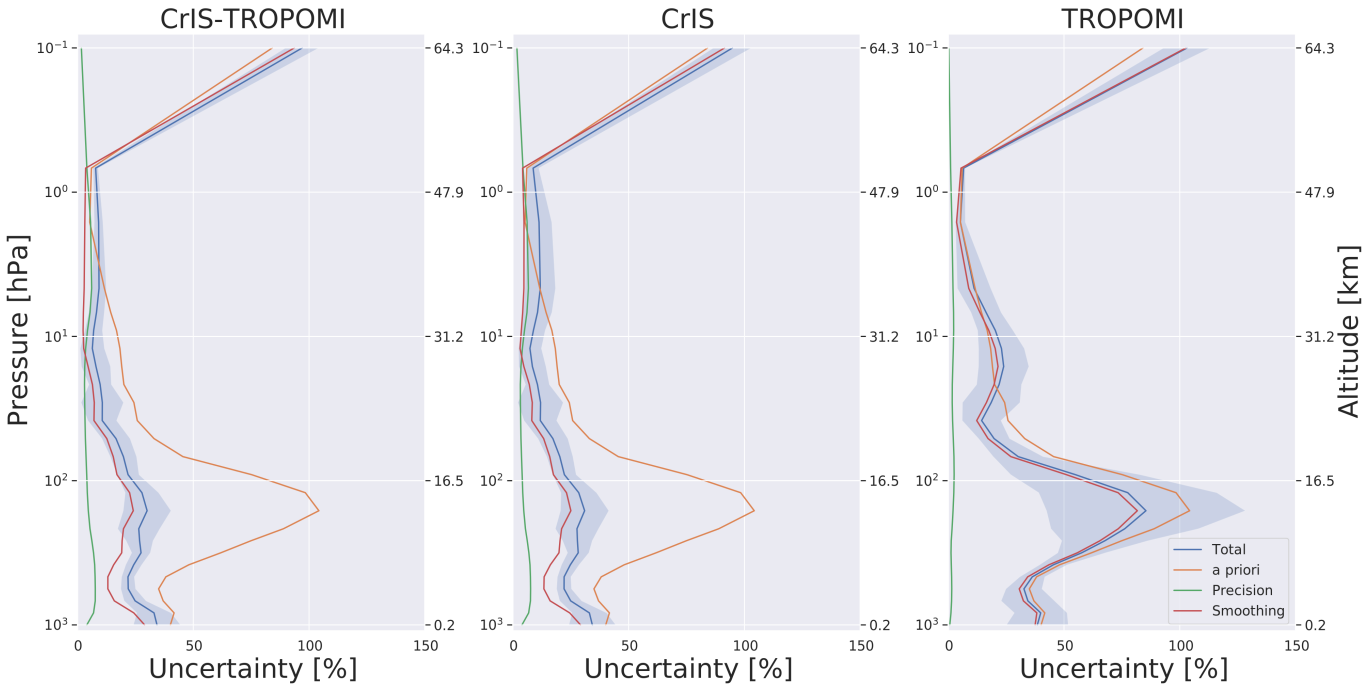

Figure 6. Retrieval uncertainty for CrIS-TROPOMI (left panel), CrIS (middle panel) and TROPOMI (right panel). Solid lines indicate the mean uncertainties on a day in August 2020, while the shaded region indicates the standard deviation of the total error. The blue line indicates the total error, the orange line shows the a priori error, the green line the measurement noise error and the red line the smoothing error.

For CrIS, total uncertainty (Eq. 7) is maximum at the surface, reducing in magnitude until the upper stratosphere (except for a local reduction in magnitude in the lower troposphere). We note that the precision errors form a small component of the total

error in the troposphere and lower stratosphere; the error budget is largely dominated by the smoothing error. Comparisons of the total uncertainty with the a priori uncertainty show a general reduction in the uncertainty, with the most reduction above the tropopause (∼100 hPa). Given that the majority of the DFS are contained within the stratosphere for CrIS (Fig. 5), this is the expected result. The ~~variability of the total uncertainty is largely consistent throughout the atmosphere, except above 10 hPa where the magnitude is lower. The~~ uncertainties shown for TROPOMI are notably larger than those shown for CrIS, with the total uncertainty indicating a minor reduction of the a priori uncertainty. This is the expected result, given that only 1 DFS is available from the TROPOMI retrieval alone. The standard deviation of the upper tropospheric retrieval is significantly larger than that of CrIS. As Fig. 4 indicates, there is very little information content for TROPOMI retrievals outside of the stratosphere, which is expected given the chosen spectral window. For the CrIS-TROPOMI retrieval, the uncertainty profile is similar to that of CrIS. The key difference is that the variability of the total uncertainty is smaller than that of CrIS, and the total/smoothing error is slightly smaller. Suggesting that the inclusion of the TROPOMI radiances reduces the uncertainty of the CrIS retrievals slightly.

3.6 Quality Assessment

Following the completion of the retrieval, the MUSES algorithm undertakes an assessment of the quality of the retrieval using a number of diagnostics (Kulawik et al., 2021). The primary quality flags are based upon the residual radiance between the calculated and observed spectra, as well as on identifying cloud contamination, based on cloud optical depth for TIR and cloud fraction for UV. The quality flags for the CrIS-TROPOMI, TROPOMI and CrIS MUSES ozone retrievals are based on a statistical analysis of small clusters of retrievals. For MUSES CrIS, this analysis made use of the significant timeline of CrIS. For MUSES TROPOMI, only subsets of retrievals have been performed; therefore, the flags are based on MUSES OMI retrievals.

For a typical day (in August 2020) consisting of roughly 40k individual retrievals, the CrIS-TROPOMI retrievals have a pass rate of 39%; the corresponding numbers for CrIS and TROPOMI are 70% and 38%, respectively. The CrIS-TROPOMI and TROPOMI failures are by large due to the presence of clouds in the sounding. The CrIS failures are primarily due to the residual radiance having too large of a magnitude.

3.7 Observation Operator

In order to directly compare the MUSES retrievals with chemical reanalysis datasets and ozonesondes, we must account for the vertical sensitivity of the MUSES retrievals. The averaging kernel and a priori can be used to construct the observation operator (Jones et al., 2003; Worden et al., 2007a):

$$\mathbf{H}(\cdot) = \mathbf{x}_a + \mathbf{A}(\mathbf{M}(\cdot) - \mathbf{x}_a), \tag{8}$$

where $\mathbf{H}(\cdot)$ is the forward transport model relating the chemical reanalysis or ozonesonde profile to the retrieval, $\mathbf{M}(\cdot)$ is the chemical reanalysis or ozonesonde profile at the location of the retrieval, and all other values are as previously defined.

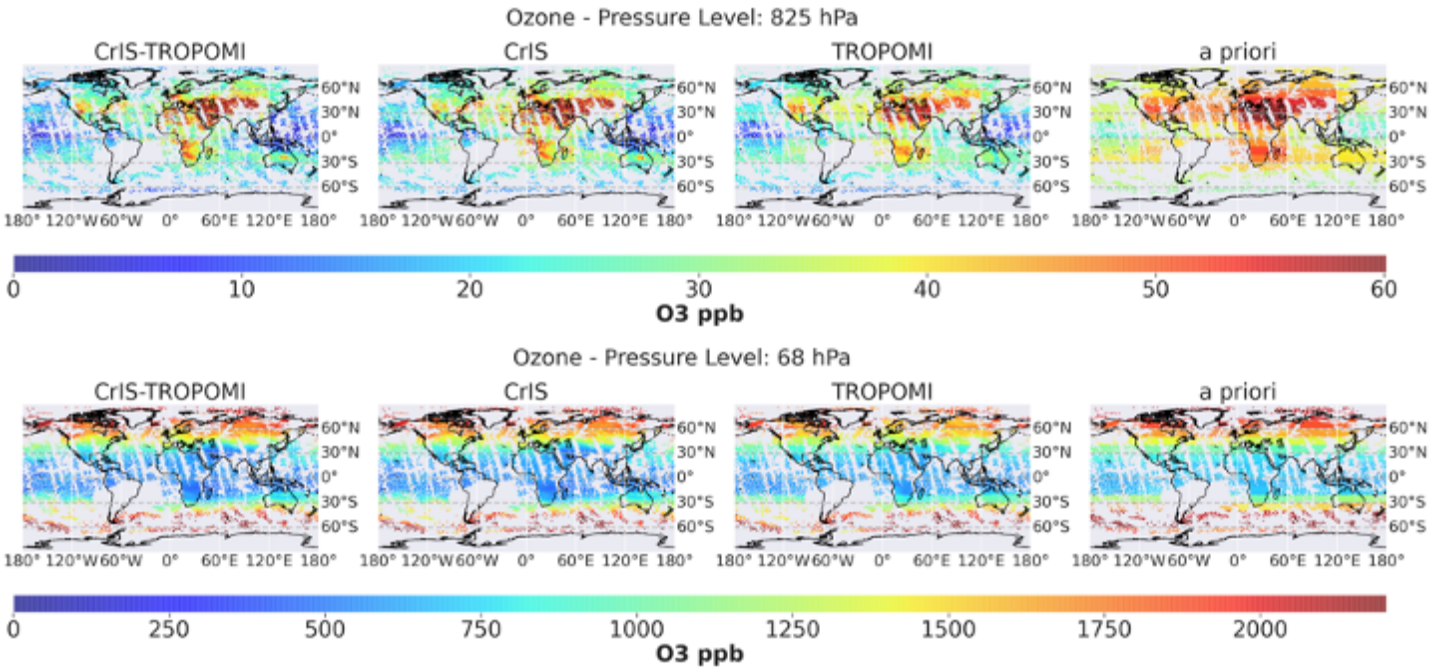

Figure 7. Global distributions of ozone on August 12 2020 in ppb, comprising of ∼10k quality retrievals. The results shown in the left hand column are from the CrIS-TROPOMI retrievals, followed by CrIS, TROPOMI and the a priori in the right hand column. Each row indicates the ozone concentrations from an example pressure level; the first row is 825 hPa, the second row is 68 hPa. These pressure levels were chosen to represent a wide range of atmospheric conditions (lower troposphere, upper troposphere and stratosphere), as well as to coincide with peaks in the CrIS-TROPOMI AK.

Side-by-side comparisons of retrievals from CrIS-TROPOMI, CrIS and TROPOMI, and the a priori on August 12 are shown in Fig. 7. The top row indicate ozone retrievals at 825 hPa (lower troposphere). The troposphere is a complex region to characterise, with the interplay of chemistry and dynamics dictating the geographic and vertical structure of ozone. The retrievals from CrIS-TROPOMI/CrIS/TROPOMI show a number of regions with significant ozone enhancements. For example, all cases show enhanced ozone in southern Africa, with some transport towards Australia. Southern Africa is dry in August and significant biomass burning occurs. Fires generate the precursors necessary to form ozone, thus yielding significant ozone over biomass burning (Sinha et al., 2004). Comparisons with the a priori show that the retrievals suggest much more localised extreme ozone enhancements, as opposed to broad low level enhancements. Other regions of enhancement highlighted (especially by CrIS-TROPOMI and CrIS) include central and east Asia. In the summertime Asia experiences a monsoon, which has a significant impact on the climate of north Africa, the middle East and Central Asia though complex interactions described elsewhere (Gettelman et al., 2004; Liu et al., 2009). The Asian monsoon has been found to enhance tropospheric ozone concentrations (Worden et al., 2009), as can be seen in the spatial maps, as well as the profile plots (Fig. C1) that indicate significant en-

hancements in the troposphere between 30°N and 50°N. Note that as shown in the AKs, there are no clear differences between CrIS-TROPOMI/CrIS-only retrievals in the troposphere. The ozone distribution at 68 hPa (stratosphere) shows the characteristics of the Brewer-Dobson circulation, with higher ozone concentrations at the poles, and lower magnitudes in the tropics. Both the 316 and 68 hPa pressure levels identify an interesting significant ozone enhancement (roughly double the surrounding regions) in the southern Indian ocean (60°S). It has been suggested that this enhancement is due to the geographical distribution of outflow from tropical convection in the upper troposphere and lower stratosphere (UTLS), which is concentrated over the southern Indian Ocean (Hitchman and Rogal, 2010). At these pressure levels, in general, the a priori and the retrievals are similar, with the key difference that the a priori does not suggest the existence of significant enhancements in the southern Indian Ocean. In general there are few obvious differences between any of the retrieval cases in the stratosphere, with minor differences in magnitude apparent.

The TROPOMI results broadly capture the identified regions of enhancement at the specified pressure levels. However, they tend to provide underestimates with respect to CrIS and CrIS-TROPOMI as a consequence of the lower DFS values in the TROPOMI retrievals, which average between 0.9 and 1 in the stratosphere, and 0 and 0.1 in the troposphere. Figs 4 and 5 show that the CrIS-TROPOMI retrievals are dominated by CrIS because of the limited well-calibrated UV bands in TROPOMI. Considering the tropospheric column results shown in the middle row, the TROPOMI results match those of the a priori, which is expected due to the limited information content (Fig. 5).

It is important to note that as a TIR instrument, CrIS is capable of retrievals at night, which TROPOMI, reliant on solar backscattered reflectances is unable to achieve. Figure 8 contrasts the night-time measurements of CrIS with those in the daytime.

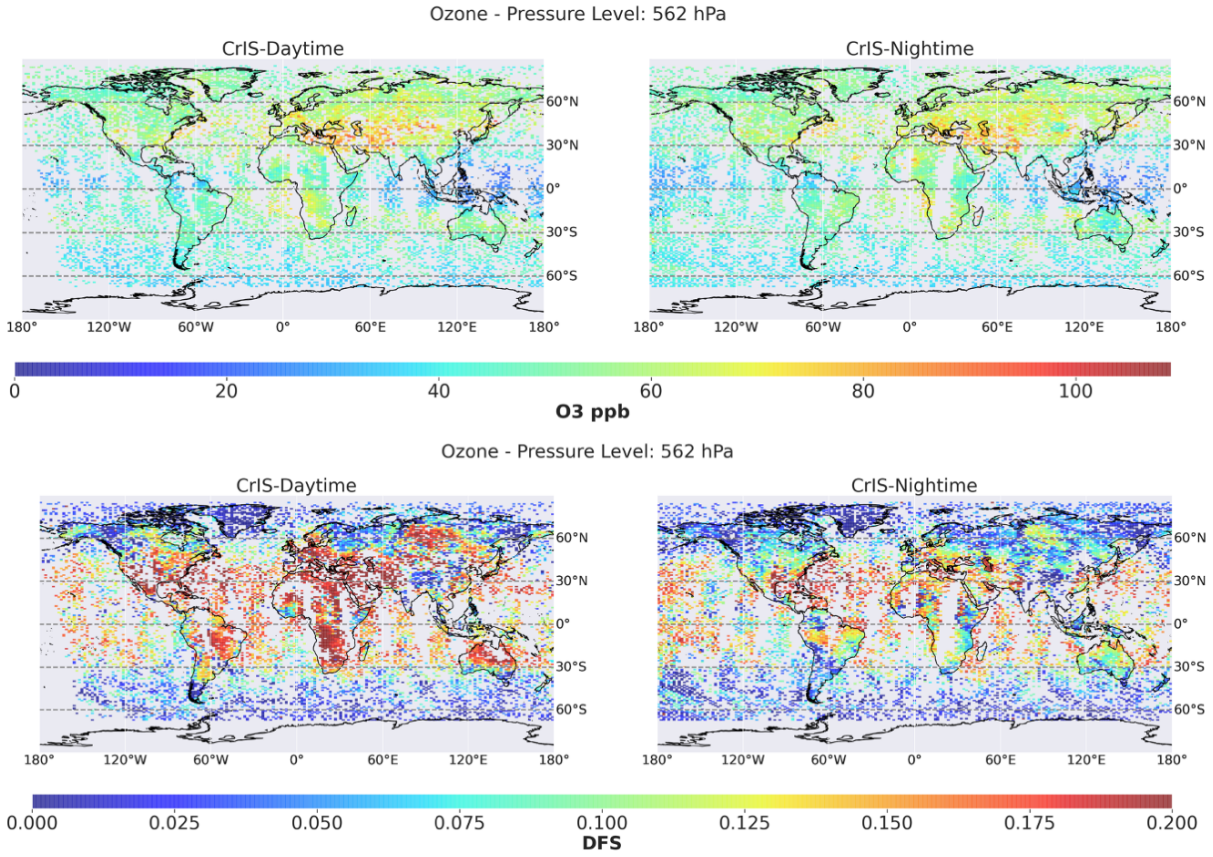

Figure 8. Top row, global distributions of ozone on August 12 2020 in ppb at 562 hPa. The results shown in the left-hand plot are daytime-only CrIS retrievals, and the right-hand plot are nighttime-only CrIS retrievals. Bottom row shows the DFS values for daytime and nighttime.

The day-time and night-time measurements are spatially consistent with some differences. For example, the daytime retrievals have a significant gap between 160°W and 180°W, while the nighttime retrievals are not available along the spine of Africa. Further, differences between the retrievals can be seen in some locations. For example, over Mongolia (∼40°N 100°E), there is at least a 50% drop in ozone concentration between the day-time and night-time cases. Some of these differences can be explained through the differences in DFS between day-time and night-time retrievals. In general we found day-time and night-time retrievals yielded similar DFS values in the sub-Arctic and Arctic regions. In the mid-latitudes and tropics, however, daytime retrievals have roughly two times greater magnitude, implying that the results should be assessed differently.

Night-time ozone measurements are currently not a topic of significant study, yet are of potential value (Tweedy et al., 2013). As with other similar plots shown in this paper, day-time/night-time retrievals are available at multiple pressure levels; the results shown in Fig. 8 are presented as an exemplar case, but are not used in the following cross comparison study.

Note that the consistent gap in retrievals over south America in Fig. 7 is due to the presence of the south Atlantic anomaly, where cosmic rays cause additional noise on the detectors, which in turn generate poor quality retrievals. This anomaly is not

apparent in the CrIS-only retrievals shown in Fig. 8. This implies that the CrIS hardware is more robust, or the TIR detectors are less sensitive to cosmic rays than the UV detectors of TROPOMI.

5 Validation and ~~intercomparison~~cross-comparison

~~All results focus on~~ In this section, we show cross-comparisons of CrIS-TROPOMI/CrIS-only/TROPOMI-only with MLS and AIRS-OMI with intense global comparisons over one day (August 12th 2020~~, for an in-depth global analysis, except for ozonesonde validation~~). In addition we provide comparisons over one or two months of the summer of 2020, with the addition of some days in different seasons for comparisons in different seasons. Validation against ozonesondes are also shown, which uses data over the course of a year.

~~Cross comparisons for additional days, focusing on August 2020, but with additional months are shown in the supplementary material~~In the previous sections of the paper we present profile retrievals of the CrIS-TROPOMI/CrIS/TROPOMI retrievals. In the following sections focus is largely placed on comparisons of column quantities, rather than focusing on specific pressure levels.

5.1 MLS

For cross-comparisons of CrIS-TROPOMI, CrIS and TROPOMI with MLS, the footprints are matched based on a distance of <1° and a time frame of <2 hours. This co-location criterion (along with AIRS-OMI) is the least stringent of all the comparisons shown in this study, due to the reduced coincidences from different satellite orbits and the relative low variability in stratospheric ozone. MLS profiles are interpolated to the MUSES pressure grid and converted to sub-columns. Only the stratospheric sub-columns are compared as the MLS data providers do not recommend the use of MLS data below 200 hPa for scientific interpretation.

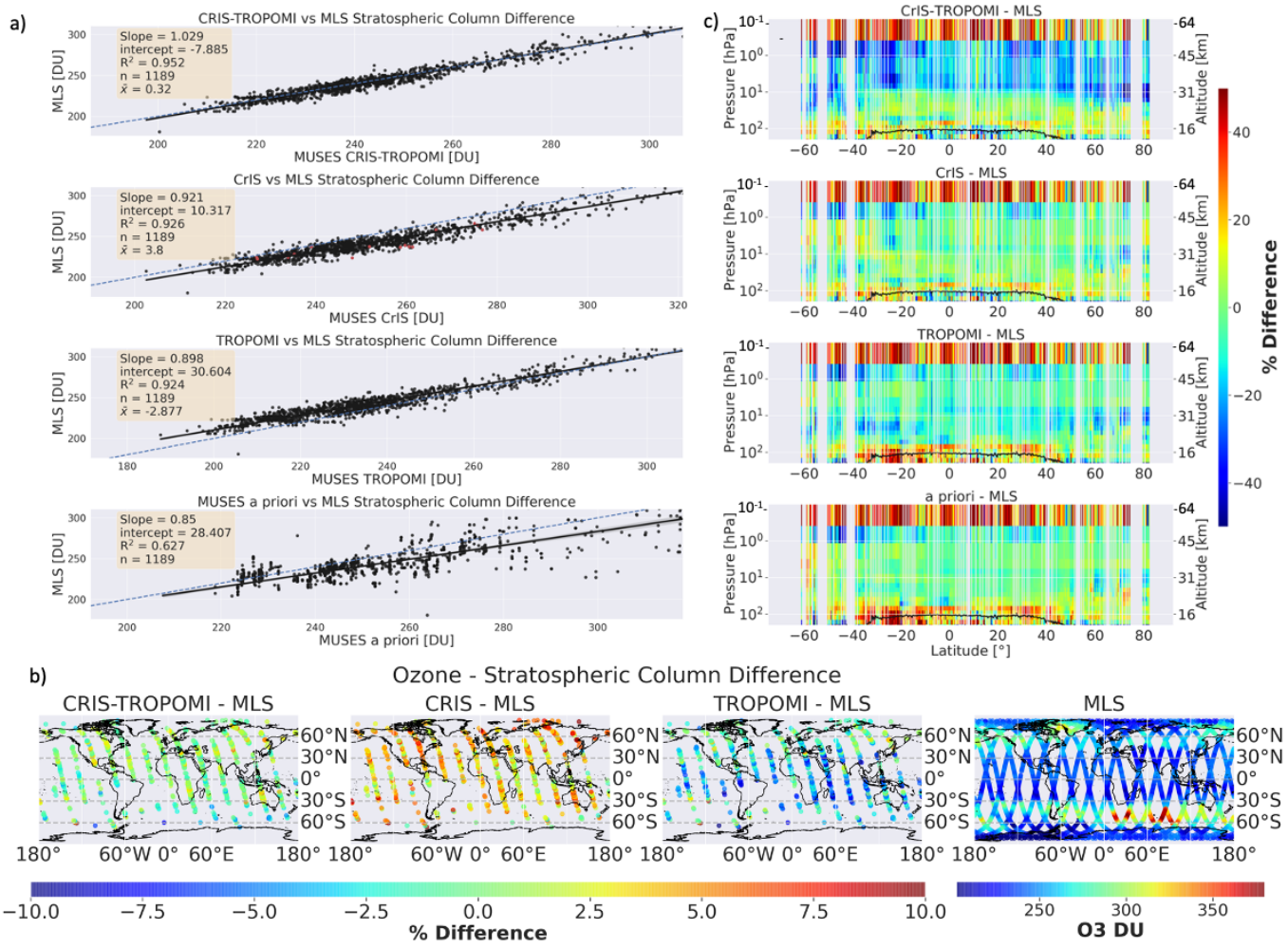

Figure 9. Cross-comparisons of MLS with CrIS, TROPOMI and CrIS-TROPOMI on August 12 2020 for the stratospheric profile. The three subplots highlighted by a) show the linear relationship between the matched stratospheric columns of MLS and, moving top to bottom, CrIS-TROPOMI, CrIS, TROPOMI and the MUSES a priori. For the CrIS plot, the black dots represent daytime retrievals, and red dots show nighttime retrievals. The linear fit statistics are indicated in the plot, showing in order the linear slope, intercept, coefficient of determination, the number of matched footprints and the mean difference between MLS and MUSES retrievals ($\bar{x}$). The second section of subplots indicated by b) shows the percentage difference between the instrument retrievals and MLS in the stratospheric column on a global grid. Moving from left to right, CrIS-TROPOMI, CrIS and TROPOMI data are shown, with the plot on the far right showing the MLS ozone stratospheric column for reference. The third section of subplots shown by c) indicates the difference between the retrieved profiles from (moving top to bottom) CrIS-TROPOMI, CrIS, TROPOMI and the MUSES a priori, compared with MLS. All values are based on the co-located points shown in a) and b) binned into one longitudinal bin, shown between 0 and 200 hPa. The black lines indicates the tropopause.

The cross-comparison results shown in Fig. 9 indicate good agreement between all instrument retrievals and MLS. Indeed, the scatter plots shown in Fig 9(a) indicate that the MLS vs CrIS-TROPOMI comparisons show especially high levels of

linearity (slope of 1.03) and correlations (R^2 of 0.952). With respect to CrIS-only retrievals, again good agreement is shown, but to a lesser degree than with respect to CrIS-TROPOMI (slope of 0.921 and R^2 of 0.926). For TROPOMI alone, while strong correlation (R^2 of 0.924) and linearity is observed (slope of 0.898), a much larger intercept is also present (30.6 DU), implying a poorer agreement when compared to intercepts seen in CrIS-TROPOMI and CrIS retrievals. A key statistic is the CrIS-TROPOMI mean difference (0.32 DU) is significantly lower than either CrIS (3.8 DU) or TROPOMI (-2.88 DU) alone, again indicating improved performance from CrIS-TROPOMI for the stratospheric column. All instrument retrievals show improved correlation over the MUSES a priori.

Considering the plots shown in Fig 9(b), the differences between MLS and CrIS-TROPOMI show a general good level of agreement (between -5 and +5%). However, there are a number of locations with larger disagreements; for example, poleward of 60°S, 10% differences are observed. For CrIS, in general a positive bias is observed across the globe, which is supported by the results from the scatter plot. Again, larger disagreements are observed below 60°S, in identical positions to those shown for the CrIS-TROPOMI comparison. For TROPOMI, larger negative biases are apparent across the globe; however, the largest biases occur in the same locations as for CrIS-TROPOMI and CrIS. However, for all three datasets, there is no obvious spatial bias, except for below 60°S. Referring to the MLS stratospheric column in Fig 9(b), we see notable anomalies in the southern hemisphere that are also captured and well represented by the MUSES retrievals (Fig 7), according to the spatial comparison points. The reference MLS plot indicates both ascending and descending node retrievals, but only descending node retrievals are compared with the MUSES data. The plots shown in Fig 9(c) indicate the differences between the datasets and MLS at each pressure level by latitude. For CrIS-TROPOMI there are mixed results with significant differences between -40 and +40% around the tropopause, which is highest pressure MLS data is usable. In the tropics, good agreement is achieved (typically in the region of 0-10%) up to 10 hPa, with greater disagreement found from the mid-latitudes up to the poles. This agreement is to be expected since the major peaks of the CrIS-TROPOMI AK are found at these pressure levels. Larger disagreement is apparent above 10 hPa, with differences up to 40% shown outside of the tropics~~. This is expected as the CrIS-TROPOMI sensitivity decreases above this pressure level, while MLS retains high sensitivity~~, that remain to be investigated. Comparisons with CrIS-only retrievals show some similar characteristics to CrIS-TROPOMI. For example, good agreement up to the 10 hPa pressure level, typically 0-10% difference, with larger disagreement towards mid-latitudes and the poles. However, above 10 hPa, while CrIS-TROPOMI shows mostly an under estimation, CrIS-only shows an over estimation with respect to MLS. Differences of between 10-40% are seen, although some examples of negative biases are also apparent, especially towards the south pole.

Following this analysis over one day, we assess the mean difference in stratospheric columns, between co-located MLS retrievals and CrIS-TROPOMI/CrIS/TROPOMI over the course of ~~August~~ several months of the summer of 2020, and several days of different seasons shown in Fig 10. Each day includes around 70 co-located retrievals, except for August 12th, where a greater data volume was processed. The results clearly show that CrIS-TROPOMI retrievals have a constant lower bias in comparison with MLS, than either CrIS or TROPOMI individually, again suggesting CrIS-TROPOMI has improved performance in the stratosphere. Note that the biases in the retrievals from the instruments over all seasons are consistent, although the magnitudes appear slightly larger outside of the summer. In addition, Fig. 10 further highlights the point shown in Fig. 9

that there is a strong likelihood that the improved performance of the CrIS-TROPOMI stratospheric column values being the result of bias cancellation in different parts of the stratosphere.

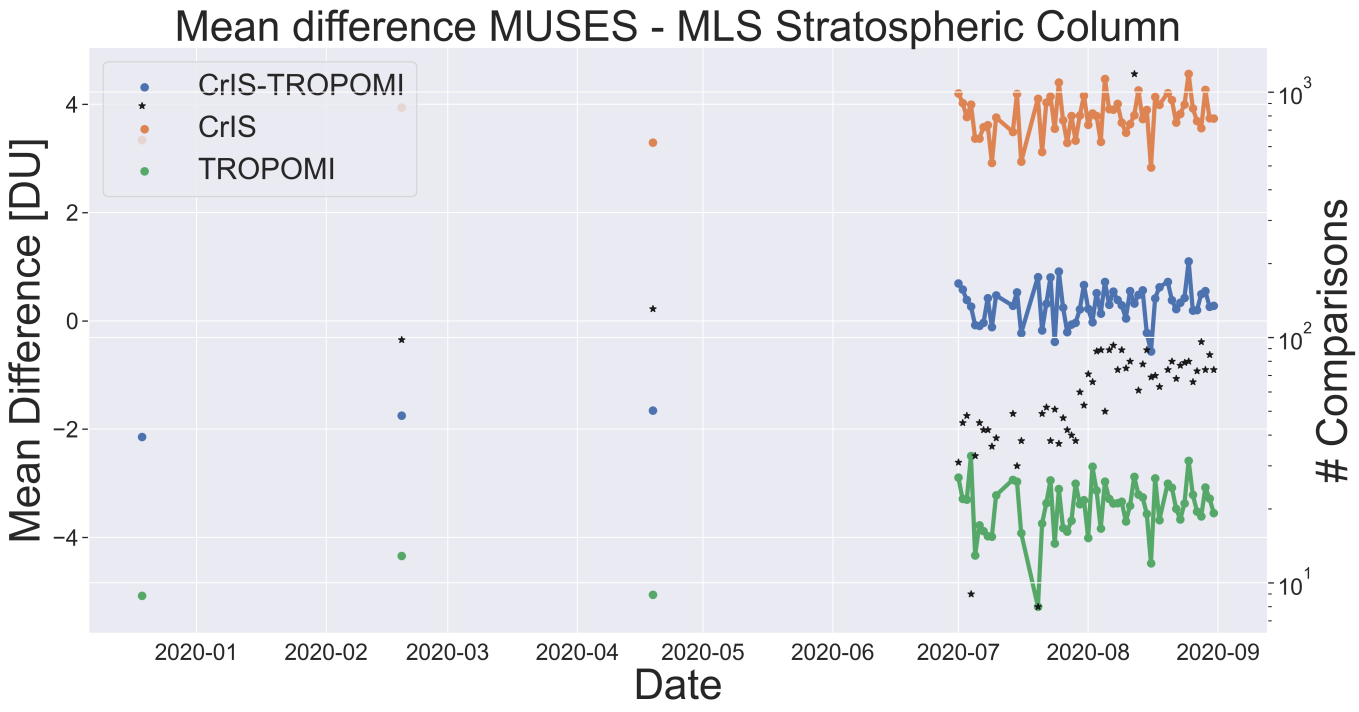

Figure 10. Global stratospheric column mean difference (in DU) between co-located MLS retrievals and CrIS-TROPOMI (blue), CrIS (orange) and TROPOMI (green) over the ~~month~~ months of July and August in 2020 and a day of December 2019, February 2020 and April 2020. The number of co-located retrievals is shown ~~in~~ by the black ~~line~~stars using the right-hand axis, which is in a log format.

5.2 AIRS-OMI

For the comparison with MUSES AIRS-OMI the CrIS-TROPOMI/CrIS and TROPOMI retrievals, as with MLS, are matched based on a distance of <1° and a time frame of <2 hours. For this cross-comparison we investigate two sub-columns, the tropospheric sub-column, Fig. 11) and the stratospheric sub-column (Fig. 12).

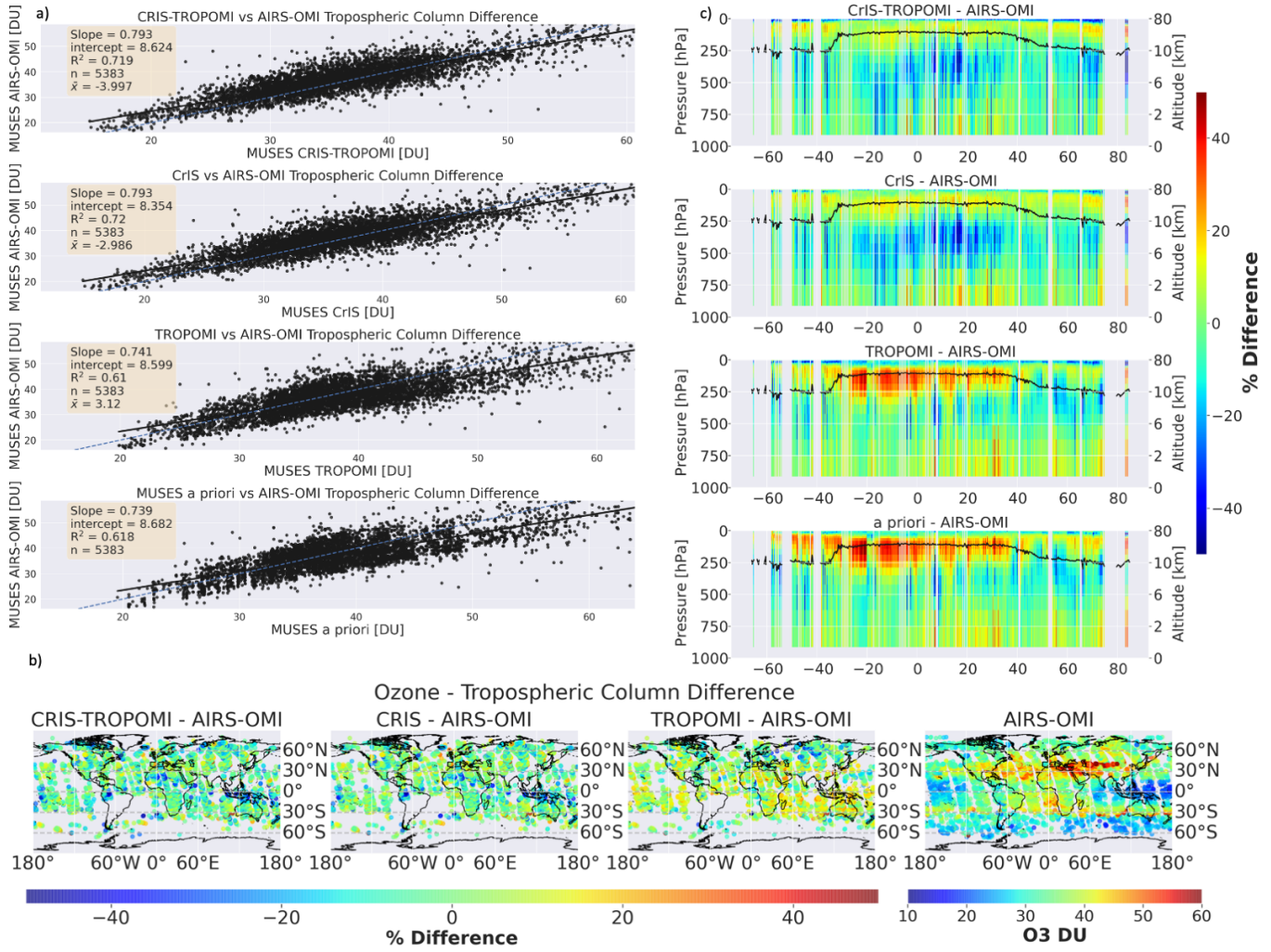

Figure 11. Cross-comparisons of MUSES AIRS-OMI with CrIS, TROPOMI and CrIS-TROPOMI on August 12 2020 for the tropospheric sub-column. The structure of the figure is as shown in Fig. 9.

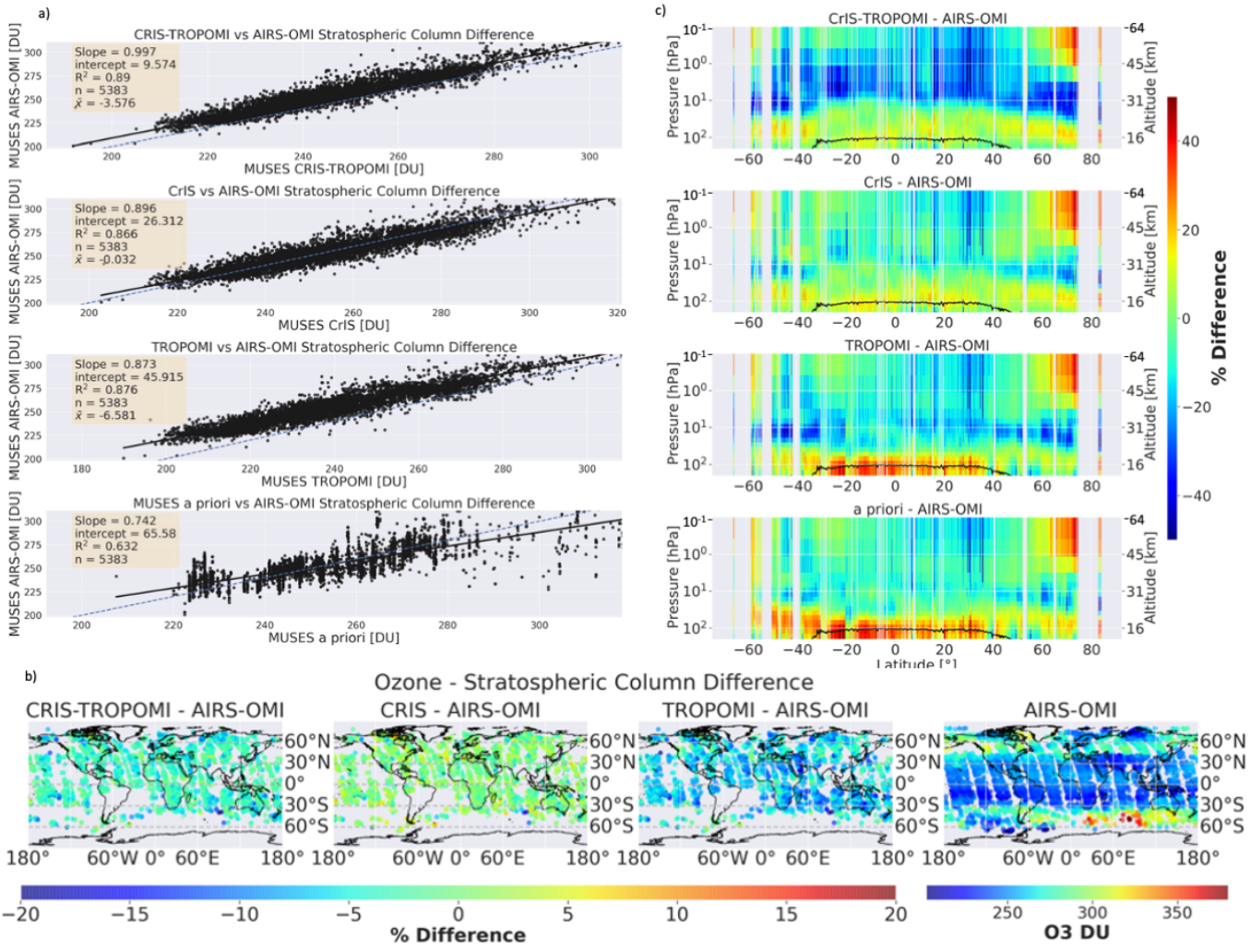

Figure 12. Cross-comparisons of MUSES AIRS-OMI with CrIS, TROPOMI and CrIS-TROPOMI on August 12 2020 for the stratospheric profile. The structure of the figure is as shown in Fig. 9, focusing on stratospheric pressure levels.

Starting with the scatter plots shown in Fig. 11(a), reasonable agreement is found between CrIS-TROPOMI/CrIS-only/TROPOMI-only and AIRS-OMI in the tropospheric column. ~~similar~~ Similar magnitudes in terms of the R^2, slope, intercept and mean difference are shown for all three comparisons, except TROPOMI-only which has a lower magnitude correlation. These scatter comparisons are shown spatially in the plots in Fig. 11(b). In general CrIS-TROPOMI, CrIS-only and TROPOMI-only show between ±20% differences across the globe, with a number of common regions showing large disagreements. For example, west Africa shows differences >40% while. The vertical profile differences between CrIS-TROPOMI/CrIS/TROPOMI and AIRS-OMI are shown in Fig. 11(c). Both CrIS-TROPOMI and CrIS have similar differences generally between -10 and 10% in the mid-latitudes through the troposphere, although there are cases with larger differences >40%. However, differences ex-

ceed 40% in the tropics. The differences in the TROPOMI profile are more significant, with up to 40% at near the tropopause in the tropics and mid-latitudes.

Stratospheric assessment of AIRS-OMI is shown in Fig. 12. Fig. 12(a) ~~indicate excellent agreement in most cases~~the overall global assessment indicates good agreement based on the shown statistics. CrIS-TROPOMI indicates a high degree of linearity (slope = 0.997), while CrIS-only and TROPOMI-only show similar linearity to a lesser magnitude. Comparable R^2 values are shown for all three cases, while the main difference is the mean difference (bias) with AIRS-OMI, where CrIS-only shows the lowest magnitude difference (-0.03), significantly lower than the other cases. The global distribution of the differences in the stratospheric profile indicated by the plots shown in Fig. 12(b) show global biases for each instrument, negative for CrIS-TROPOMI and TROPOMI, and positive for CrIS. There is also some indication that larger biases occur at regions with significant differences from the regional mean, e.g., the southern Indian Ocean. The differences in the stratospheric profile, highlighted by the subplots in Fig. 12(c), are more pronounced than those in the tropospheric profile. CrIS-TROPOMI results show between 20 and 40% difference between 10 and 1 hPa across a wide range of latitudes, dropping to <10% above this point, contrasting the overall results shown in (a). CrIS, in contrast, indicates a largely uniform ∼10% difference above the 60 hPa level, with a number of notable exceptions, e.g., 19°. TROPOMI shows a different pattern, showing large (at least 40%) differences in the mid-latitudes between 1 and 20 hPa. However theses differences are lower around the tropics.

5.3 ~~GODFIT OFFL TROPOMI TOC product~~

~~The GODFIT product uses the same Huggins band so that differences between the MUSES product should be attributable to retrieval methods and models.~~

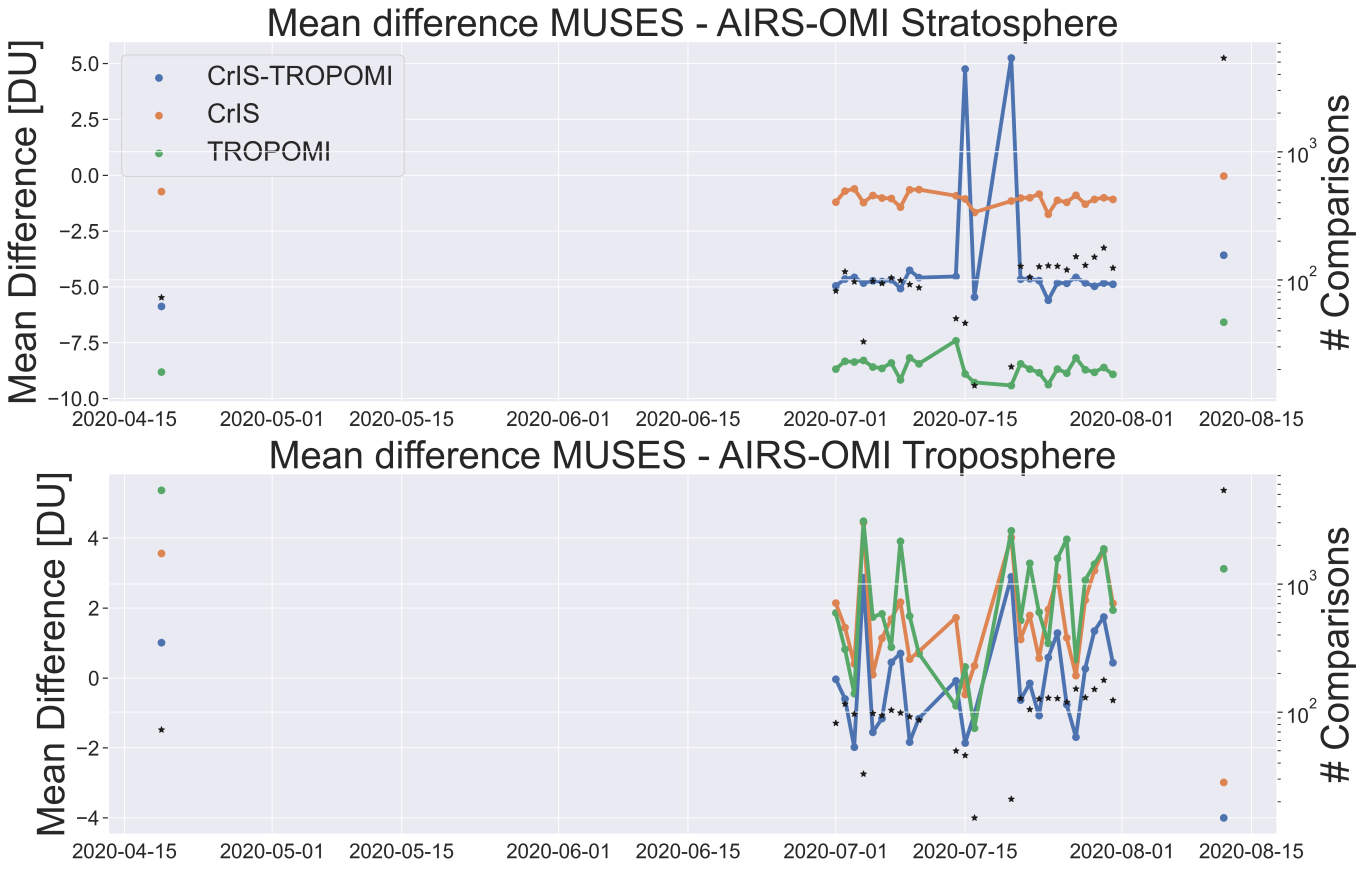

Figure 13. ~~Cross-comparisons of TROPOMI OFFL GODFIT TOC product~~ As Fig 10, however with ~~MUSES TROPOMI TOC on August 12 2020. Comparisons of~~ the ~~MUSES retrieved product with the GODFIT product indicated in the~~ top panel ~~, comparisons with the~~ focusing AIRS-OMI vs MUSES ~~a priori columns shown~~ retrievals in the stratospheric column, and the bottom panel focusing on the tropospheric column for the same comparisons. Comparisons for July 2020 are shown, with additional days in April and August also shown.

~~Fig. ?? show high correlation (R^2=0.93) and a near unity slope (1.04) with a small positive bias of about -2.8 DU, which is <1% of the TOC. These differences are attributable in part to optimal estimation approach used in the MUSES profile retrieval versus the total column fit in the GODFIT algorithm. Both show that restricting the retrieval to the Huggins band limits TROPOMI to a total ozone column.~~

~~A significant improvement, both in terms of bias and correlation is apparent when the GODFIT product is compared against the MUSES retrieval product, as opposed to the MUSES a priori.~~

5.3 ~~Chemical reanalysis~~

~~The following subsection contains the comparison between the chemical reanalyses CAMS and MOMO-Chem against the CrIS-TROPOMI/CrIS/TROPOMI retrievals. These reanalyses have distinct advantages over the other comparison sources used~~

in this paper. These include high spatial and temporal resolution ozone profiles, not limited in vertical sensitivity, while at the same time taking advantage of the observations of numerous satellite instruments. However, these reanalysis datasets are not validation sources, and areas of disagreement should be considered as a point for further discussion and evaluation.

The criteria for this co-location are spatial differences of <0.5°, and temporal differences of <2 hours, the temporal resolution of the chemical reanalysis. The observation operator identified in Eq. 8 is then applied to the co-located reanalysis profiles.

5.2.1 CAMS Reanalysis

Cross-comparisons of CAMS-reanalysis with CrIS, TROPOMI and CrIS-TROPOMI on August 12 2020 for the tropospheric sub-column. The layout of this figure is as Fig. 11.

Fig. **??**(a) shows good agreement of the CAMS-reanalysis with CrIS-TROPOMI The time-series shown in Fig 13 is generally consistent with the results indicated in Figs 12 and CrIS-only results. CrIS-only has a slightly better agreement with a closer linear relationship (slope of 0.851 vs slope of 0.827), higher correlation (R^2:0.785 vs 0.757) and a lower mean difference. TROPOMI-only, however, shows the best agreement of all three instruments. This initially runs counter to the results shown in Figs. 9 and 11. Yet, considering Eq. 8, when using the TROPOMI AK, (which based on Fig. 4 is effectively 0 in the troposphere), the term $\mathbf{H}(\cdot)$ is effectively equivalent to the a priori with only minor TROPOMI sensitivity in the troposphere. Therefore when comparing the TROPOMI tropospheric retrievals against CAMS tropospheric column modified by the observation operator what is actually being compared is the TROPOMI sub-column and a slightly modified a priori sub-column. These two quantities are going to be very similar, hence the close results shown in Fig. **??**. This was confirmed when we compared the TROPOMI-only tropospheric column results against CAMS unmodified by the observational operator, given the a priori and TROPOMI-only tropospheric column show almost identical comparisons.

For CrIS-TROPOM/The stratospheric column differences between the MUSES retrievals and AIRS-OMI show CrIS-only retrieval datasets, CAMS overestimates with respect to MUSES, especially for larger or lower magnitude retrievals where more scatter can be observed. Considering the spatial plots shown in Fig. **??**(b), we note that while there are numerous locations where the MUSES datasets individually disagree with CAMS, CrIS-TROPOMI/CrIS-only show multiple instances of >20% difference in large ocean bodies, e.g., the Pacific. Building on this, both Fig. 7 and Fig. **??** show low ozone concentrations in south east Asia. The tropospheric profile results shown in Fig. **??**(c) indicate good agreement between CAMS and CrIS-TROPOMI/CrIS-only across most latitudes, with differences <5%, apart from between 0 and 20° where >20% difference is observed. These differences match in location with south East Asia identified in Fig. **??**(b). Other sources of disagreement are focused on the tropopause in the tropics, and at high latitudes for CrIS-TROPOMI, with >20% differences. Plots b) and c) highlight the disagreement between CAMS and the MUSES retrieval in Tropical regions, the causes of these differences should be investigated in future work.

Fig. **??** shows the differences in the stratospheric sub-column. Starting with the scatter plots in Fig. **??**(a), all three instruments perform well. CrIS-TROPOMI and CrIS show similar levels of linearity based on the slope and intercept values, although CrIS has slightly improved performance, while CrIS-TROPOMI has higher correlation (R^2=0.936 vs 0.911) and lower mean difference (-1.55 vs 2.06). TROPOMI does not agree as well as either of the other datasets, but retains a strong correlation

(R^2=0.93). All datasets show improvements over the a priori. Fig. **??**(b) shows that CrIS-TROPOMI largely exhibits a minor negative bias, with some examples of large negative biases towards Antarctica, which is replicated by CrIS-only and TROPOMI-only results. CrIS-only, meanwhile, largely exhibits a positive bias across the globe, with few areas of significant disagreement. TROPOMI-only shows a negative bias spread across the globe, ranging from 0 to >20%. Key areas of disagreement include the Indian and Pacific oceans. For the profile differences shown in Fig. **??**(c), CrIS-TROPOMI generally indicates good agreement (typical difference <10%), with exceptions in with the 10-1 hPa range in the mid-high latitudes, where disagreements of ~20% are observed. CrIS-only shows a larger positive bias, typically >10% above 10 hPa, that remains fairly constant across all latitudes, while indicating similar levels of bias as lowest mean bias, followed by CrIS-TROPOMI about the tropopause. TROPOMI-only generally indicates good agreement through the stratosphere; however, there are some regions of significant differences , most notably towards Antarctica, where differences greater than 40% are observed through multiple pressure levels.

5.2.1 JPL MOMO-Chem

As with using different satellite retrievals for satellite inter-comparisons, we use two chemical reanalysis datasets to provide a wide ranging assessment of the accuracy of CrIS-TROPOMI retrievals. The reanalysis datasets themselves show substantial disagreements. MOMO-Chem, unlike the CAMS-reanalysis, optimises the precursor emissions of ozone, as well as ozone itself.

Cross-comparisons of JPL MOMO-Chem with CrIS-TROPOMI, CrIS and TROPOMI for the tropospheric column level on August 12 2020. The structure of the figure is the same as shown in Fig. **??**.

Fig. **??**(a) shows excellent agreement between CrIS-TROPOMI and CrIS-only and TROPOMI-only. These differences are true in the results shown in April, July and August, with MOMO-Chem in terms of linearity. The linearity, and the mean difference bias of the comparisons are better than those shown with the CAMS cross-comparison (Fig. **??**), however the R^2 values which are very similar. The implication from these comparisons is that both MOMO-Chem and CAMS capture the same enhancements as the MUSES retrievals, but there is less bias between MOMO-Chem and MUSES, as opposed to CAMS, in the troposphere. As with CAMS, TROPOMI comparisons with MOMO-Chem in the troposphere are not relevant when a satellite operator is applied. The spatial distribution of differences indicated in the panels under Fig. **??**(b) show some similar patterns of agreement/disagreement for CrIS-TROPOMI/CrIS. In the northern hemisphere, there are large regions with significant negative biases, with differences up to 40%. In the southern hemisphere, a general positive bias is shown (~20%), with fewer locations with larger disagreement. Comparisons with the MOMO-Chem panel show that the major disagreements occur where MOMO-Chem indicates significant enhancements over oceans, e.g., the Atlantic ocean (0-30°N, 0-30°W. Indeed, the AIRS-OMI (Fig. 11) and the CrIS-TROPOMI/CrIS/TROPOMI retrievals (Fig. 7) do not suggest the presence of significant enhancements in the Atlantic ocean, making this a key point of disagreement between the satellite retrievals and the reanalysis estimations. We further note that the tropospheric ozone concentrations are significantly larger than those indicated by CAMS, highlighting a point of contention between the two reanalysis datasets. The tropospheric differences indicated by the plots shown in Fig. **??**(c) show very similar results for CrIS-TROPOMI and CrIS. Good agreement (<10% difference) is found in the

~~northern hemisphere above 40° and in the tropical southern hemisphere. Worse agreement is found in the northern hemisphere tropics to mid-latitudes (up to 40% differences), caused by the disagreement in the Atlantic. Poor agreement is also found below 40°S in the upper troposphere, with differences between 20-40%. It is interesting to note that both CAMS and MOMO-Chem show specific latitudes of disagreement, in the tropics for CAMS, and northern hemisphere mid-latitude for MOMO-Chem. In summary for the troposphere, good agreement is found between MOMO-Chem~~ some changes in magnitude, and outliers with CrIS-TROPOMI in July. For the tropospheric trends the differences are less obvious, and ~~CrIS-only, although disagreement is found in regions of outflow. The improved comparisons of MOMO-Chem in the troposphere over the CAMS-reanalysis, highlighted by the improved linearity in MOMO-Chem, points to the importance of assimilating ozone precursors into the reanalysis and the potential value of direct tropospheric ozone assimilation.~~

~~The MOMO-Chem reanalysis is primarily aimed at assessing tropospheric ozone. While the reanalysis levels do extend into the stratosphere, they are relatively limited with respect to~~ there are clear differences in terms of the ~~CAMS-reanalysis and the MUSES retrieval grid. Therefore for this study we only focus on tropospheric ozone from MOMO-Chem.~~ magnitude, in the results shown in July, and those shown in April and August. However, note in general more positive bias in CrIS-only and TROPOMI-only, as opposed to CrIS-TROPOMI.

5.3 Ozonesondes

Validation of CrIS-TROPOMI/CrIS/TROPOMI retrievals with the ozonesondes was performed from September 2019 to August 2020 and split into seasons (Fall/Winter/Spring/Summer). The ozonesonde validation includes 105 separate ozonesonde soundings, and 3541 individual satellite intercomparisons, based on co-location criteria of <100 km. The MUSES observation operator has been applied following Sec. 3.7 in order to account for vertical sensitivity.

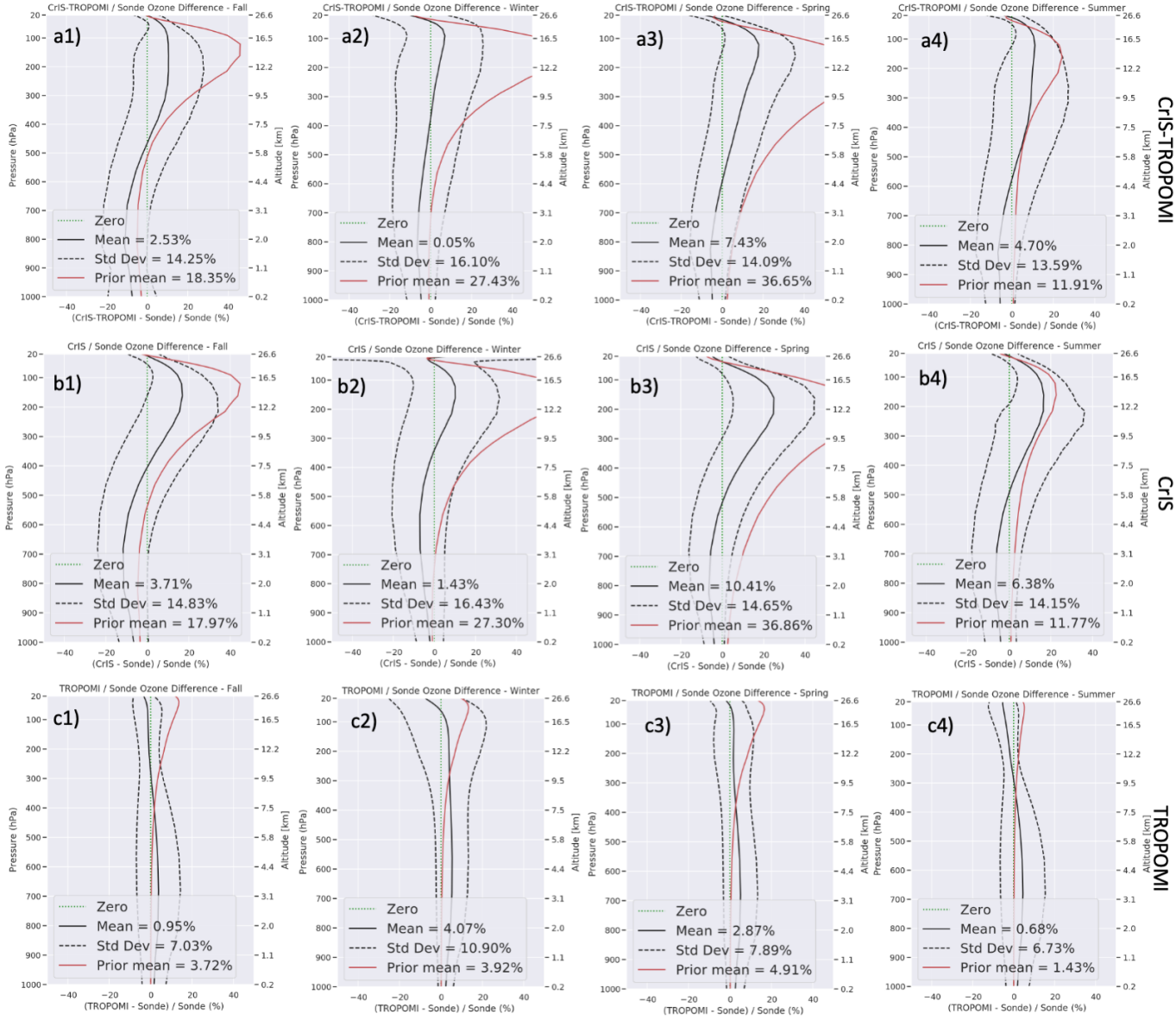

Figure 14. Ozonesonde comparisons MUSES CrIS-TROPOMI, CrIS and TROPOMI ozone retrievals. The columns represent the comparisons over different seasons (1=Fall, 2=Winter, 3=Spring, 4=Summer), the rows represent the instrument comparisons (a=CrIS-TROPOMI, b=CrIS, c=TROPOMI). The solid black lines are the mean difference, the dashed black lines are $\pm 1\sigma$, the red line is the apriori profile and the dashed green line is the zero line, these values for the tropospheric columns are indicated on the plots.

Table 8 Global statistical comparisons between CrIS-TROPOMI/CrIS/TROPOMI and ozonesondes with satellite observation operator applied over a 12 month period in 2019/2020. Analysis is at the pressure levels 681, 464 and 316 hPa.

Pressure Level	Metric	Fall			Winter			Spring			Summer		
		CrIS-TROPOMI/ CrIS/TROPOMI			CrIS-TROPOMI/ CrIS/TROPOMI			CrIS-TROPOMI/ CrIS/TROPOMI			CrIS-TROPOMI/ CrIS/TROPOMI		
681 hPa	Mean (ppb)	-5.62	-6.63	2.37	-3.13	-3.92	2.72	-1.25	-2.64	2.69	-1.43	-2.65	2.54
	Mean (%)	-10.7	-13.0	4.39	-6.13	-7.96	5.26	-2.26	-5.55	5.11	-2.69	-5.10	4.97
	RMS (ppb)	8.70	9.51	6.16	8.07	7.53	4.95	5.91	5.87	5.38	6.16	6.65	6.03
	RMS (%)	16.4	18.8	11.5	15.1	15.0	9.21	12.2	12.0	9.72	12.3	13.0	11.3
464 hPa	Mean (ppb)	0.155	-2.89	1.79	-1.57	-3.64	2.83	2.00	1.58	2.20	3.06	0.606	2.49
	Mean (%)	-0.154	-5.67	2.99	-2.34	-6.72	5.07	4.91	3.01	3.83	6.17	1.67	4.24
	RMS (ppb)	8.21	9.29	5.73	10.0	10.0	5.46	6.79	7.73	5.16	9.14	8.16	6.34
	RMS (%)	13.7	16.2	9.55	16.3	17.2	9.44	14.3	14.2	8.42	16.3	14.3	10.3
316 hPa	Mean (ppb)	4.96	4.53	0.598	-0.615	-0.09	3.09	5.09	9.78	1.68	5.39	6.50	1.78
	Mean (%)	7.21	5.97	0.954	-0.874	-0.325	4.26	9.41	15.9	2.16	9.56	11.0	2.52
	RMS (ppb)	10.6	11.68	4.14	13.6	22.6	7.81	11.4	17.3	6.50	13.0	13.3	5.91
	RMS (%)	15.2	15.9	6.10	19.1	19.5	10.7	17.8	23.5	7.74	19.5	20.5	7.99
Troposphere	Mean (%)	2.53	3.71	0.95	0.05	1.43	4.07	7.43	10.4	2.87	4.70	6.38	0.68
R^2 Troposphere		0.99	0.99	0.99	0.97	0.97	0.99	0.98	0.99	0.99	0.99	0.99	0.99
Number of profiles		25			32			20			28		
Number of satellite inter-comparisons		745			1324			551			921		

The results shown in Fig. 14 generally indicate a negative bias in the lower troposphere and a positive bias in the upper troposphere for CrIS-TROPOMI and CrIS. There are numerous outliers apparent, especially in winter with a large negative bias in the upper troposphere. For the winter cases, the upper troposphere bias is less apparent due to these negative outliers. Focusing on the results for TROPOMI, only a minor mean bias is observed through the troposphere, which can be explained due to the lack of TROPOMI sensitivity in the troposphere.

Table 8 quantifies the comparisons shown in Fig. 14. ~~As with the comparisons with CAMS and MOMO-Chem, the~~ The low information content of TROPOMI in the troposphere means the application of Eq. 8 yields the TROPOMI precision. When calculating the difference between the TROPOMI profile (which in the troposphere is a noisy replication of the a priori) and the modified ozonesonde profile, the remainder is the TROPOMI precision. Meaning the TROPOMI/ozonesonde comparison

is a useful assessment of the predicted TROPOMI precision. According to Fig. 6, TROPOMI precision is typically <5%, which roughly matches the values indicated in Table 8. In general, when compared to the AIRS-OMI/ozonesonde comparisons identified in Fu et al. (2016), we see similar levels of deviations and differences. For example, at 316 hPa in winter, AIRS and OMI have a mean difference between 15-22%, while AIRS-OMI has a difference of 7.7%. CrIS-TROPOMI and CrIS-only show differences of 9-11% at this pressure level. The percentage RMS difference for CrIS-TROPOMI/CrIS-only is generally lower than for AIRS-OMI/AIRS/OMI. Suggesting CrIS-TROPOMI/CrIS-only have comparable or improved performance in the troposphere. We note that the comparisons of ozonesondes to CrIS-TROPOMI and CrIS-only have similar results across all seasons, and especially in the RMS values, although there are exceptions to this (e.g., Spring at 316 hPa). This highlights the similar performance, but also indicates the limited impact of TROPOMI on the CrIS-TROPOMI product in the troposphere, with AIRS-OMI showing a marked improvement from a combination of AIRS and OMI in most cases. However, the majority of results shown in Table 8 do indicate that CrIS-TROPOMI performs slightly better than CrIS-only, especially in Autumn. Consequently, the joint retrieval can give improved performance in the troposphere.

Table 9 shows comparisons of CrIS-TROPOMI/CrIS/TROPOMI against ozonesondes without the satellite operator applied. This allows for comparisons of instruments with differing sensitivities (i.e. CrIS and TROPOMI), meaning the instrument with the best sensitivity should show the closest agreement with the ozonesondes. The results in Table 9 show CrIS-TROPOMI generally as the best performing instrument, except in Winter when CrIS is generally superior. As expected, TROPOMI in almost all cases is the worst performing.

Table 9 As Table 8, but showing comparisons with ozonesondes without satellite observation operators applied.

Pressure Level	Metric	Fall			Winter			Spring			Summer		
		CrIS-TROPOMI/ CrIS/TROPOMI			CrIS-TROPOMI/ CrIS/TROPOMI			CrIS-TROPOMI/ CrIS/TROPOMI			CrIS-TROPOMI/ CrIS/TROPOMI		
681 hPa	Mean (ppb)	-3.41	-4.40	1.24	0.805	0.180	6.25	-2.26	-3.68	6.35	-2.31	-3.56	3.56
	Mean (%)	-5.17	-6.91	4.58	2.92	1.27	14.6	-4.44	-7.54	12.9	-0.42	-2.83	13.1
	RMS (ppb)	9.24	10.7	10.9	9.45	9.14	11.7	7.21	8.06	9.68	10.9	11.4	12.9
	RMS (%)	16.4	18.7	20.3	20.0	19.3	25.8	14.7	16.2	20.4	25.2	25.3	36.3
464 hPa	Mean (ppb)	0.303	-2.81	2.34	0.983	-1.34	6.94	-0.977	-1.50	9.68	0.995	-1.55	5.25
	Mean (%)	4.58	-0.940	9.22	3.26	-1.39	16.9	-1.29	-3.17	19.7	5.09	0.496	15.8
	RMS (ppb)	14.2	14.8	15.2	11.6	11.8	14.3	8.86	10.7	12.3	13.0	12.9	16.6
	RMS (%)	25.5	24.6	27.8	22.4	22.1	30.7	16.2	18.3	24.6	23.9	22.5	35.1
316 hPa	Mean (ppb)	0.679	0.214	4.82	-2.07	-1.23	8.90	7.45	11.9	24.6	4.70	5.82	11.0
	Mean (%)	2.83	1.74	10.8	1.78	2.89	26.8	17.8	24.2	56.2	8.99	10.5	24.3
	RMS (ppb)	12.4	13.7	11.4	22.1	23.6	25.7	17.8	21.3	35.2	16.4	17.5	20.5
	RMS (%)	19.6	21.1	23.4	31.4	34.3	50.5	33.9	40.8	70.6	24.1	25.9	42.0

5.4 Summary of Validation and Cross-comparison

The results shown in this paper and the supplementary material shows that CrIS-only agrees well with all datasets compared against it, both in the troposphere and the stratosphere. The addition of the short TROPOMI window to form CrIS-TROPOMI, improves comparisons against MLS ~~in the stratosphere, with all results shown in the main paper and the supplementary material having the lowest mean difference bias of CrIS-TROPOMI/CrIS/TROPOMI. Differences between CrIS-TROPOMI and CrIS-only are less clear in other stratospheric comparison cases, however, differences with CAMS and MOMO-Chem raise interesting scientific questions for further analysis~~stratospheric columns, although challenges remain for stratospheric profile comparisons, requiring further investigation. Comparisons with satellite data and reanalysis in the troposphere do not show clear differences between CrIS and CrIS-TROPOMI, however, CrIS-TROPOMI shows better performance than CrIS-only against ozonesondes, which is indicative of improved performance in the troposphere through joining CrIS and TROPOMI.

6 Discussion

6.1 Investigating Windows 1 and 2 for TROPOMI in the context of CrIS

This study has focused on a small window within UVIS of TROPOMI; however, as shown in Mettig et al. (2021), UV1 & UV2 of TROPOMI provide substantially more information than UVIS, but suffer from significant calibration challenges. In this section we investigate the potential information content of using UV1 & UV2 in combination with MUSES CrIS retrievals. For this purpose, we calculate AKs (as shown in Fig. 4 over a combination of UV1 & UV2 (270-330 nm) and UV2 alone (300-330 nm), assuming perfect calibration accuracy. We also only run the forward model to generate these AKs, which causes a minor disparity between the CrIS DFS values in this analysis, and those shown in Fig. 4. The first row of Fig. 15 shows the combination of UV1 & UV2 with CrIS, as well as CrIS and TROPOMI on their own. These results indicate a significant boost in information content over the whole profile when compared to those shown in Fig. 4. TROPOMI alone accounts for 5.3 DFS in the profile, as opposed to 1 in this study. The joint profile shows the characteristics of TROPOMI in the stratosphere, but retains some of the characteristics of CrIS in the troposphere. We note that the DFS in the troposphere show an improvement over that of CrIS alone (1.9 from 1.5), suggesting that a DFS boost of more than 25% in the troposphere is gained through the combination of CrIS and TROPOMI.

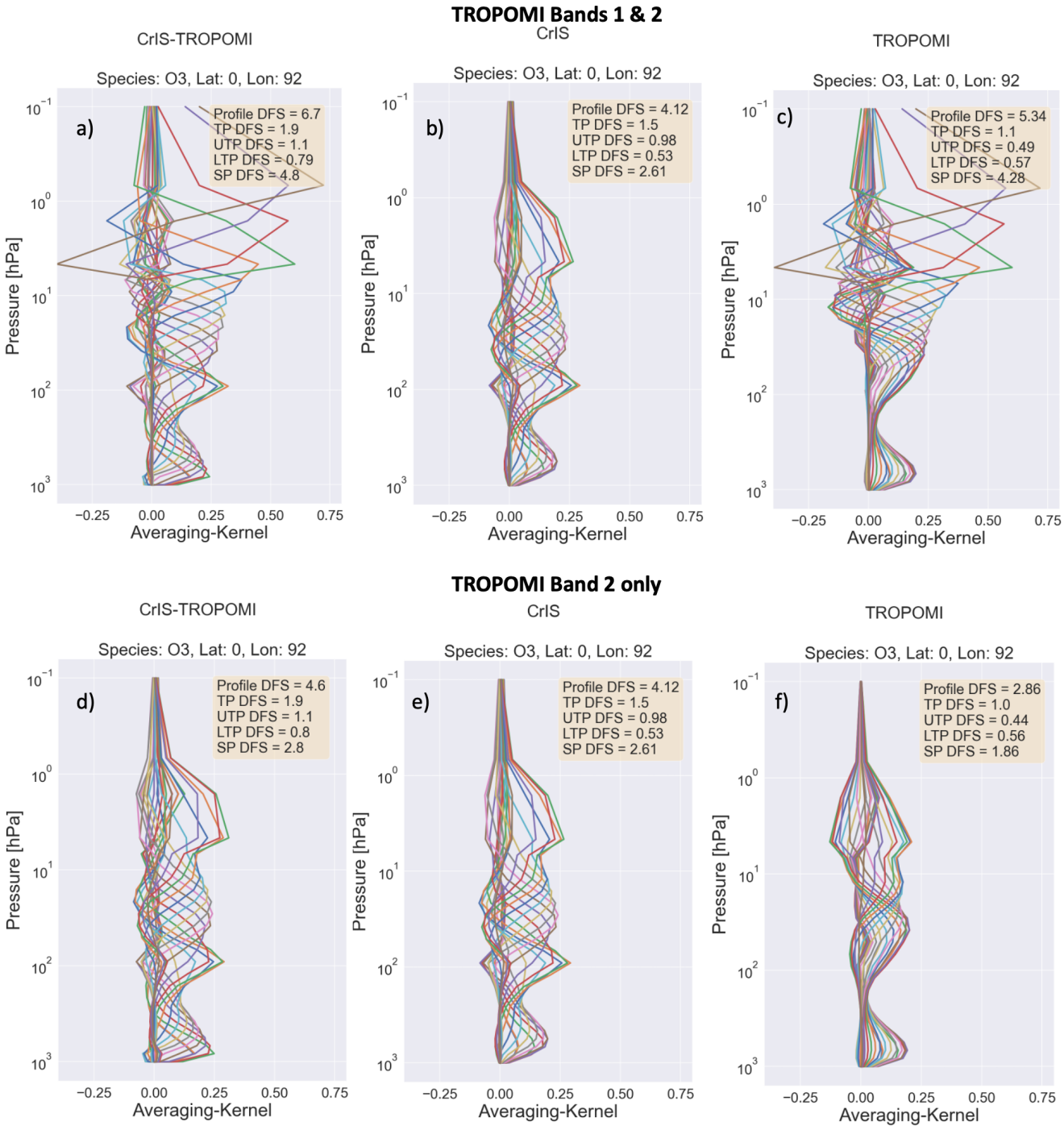

Figure 15. Example theoretical AKs comparisons, the top row shows CrIS-TROPOMI using UV1 & UV2 of TROPOMI (a), compared to CrIS (b) and UV1 & UV2 of TROPOMI (c). The second row shows the same comparison, but only using UV2 of TROPOMI. DFS values for the total profile as well as separate sub-columns are indicated in each plot for comparison purposes.

Building on this assessment, investigations have been held into the CrIS-TROPOMI UV1 & UV2 combination (Mettig et al., 2022). This research has found, as suggested in Fig. 15, that a significant boost to the information content is achieved by this combination. However, the CrIS retrieval in this work has a substantially different AK to that presented in this paper, as well as different a priori and ancillary inputs, suggesting ~~that a future MUSES joint CrIS-TROPOMI UV1 & UV2 retrieval will differ from this work~~room for further investigation.

6.2 TROPOMI UVIS

Zhao et al. (2021) evaluate and discuss the use of a window within UVIS of TROPOMI (314-340 nm) for ozone retrievals. It was found that while UVIS is adversely affected by calibration issues, these are not as significant as those indicated in UV1 & UV2. Therefore, future steps will be to use the TROPOMI 314-340 nm window for the joint retrieval, once corrected for any calibration issues. The potential information content of this CrIS-TROPOMI UVIS window is shown in Fig. 16.

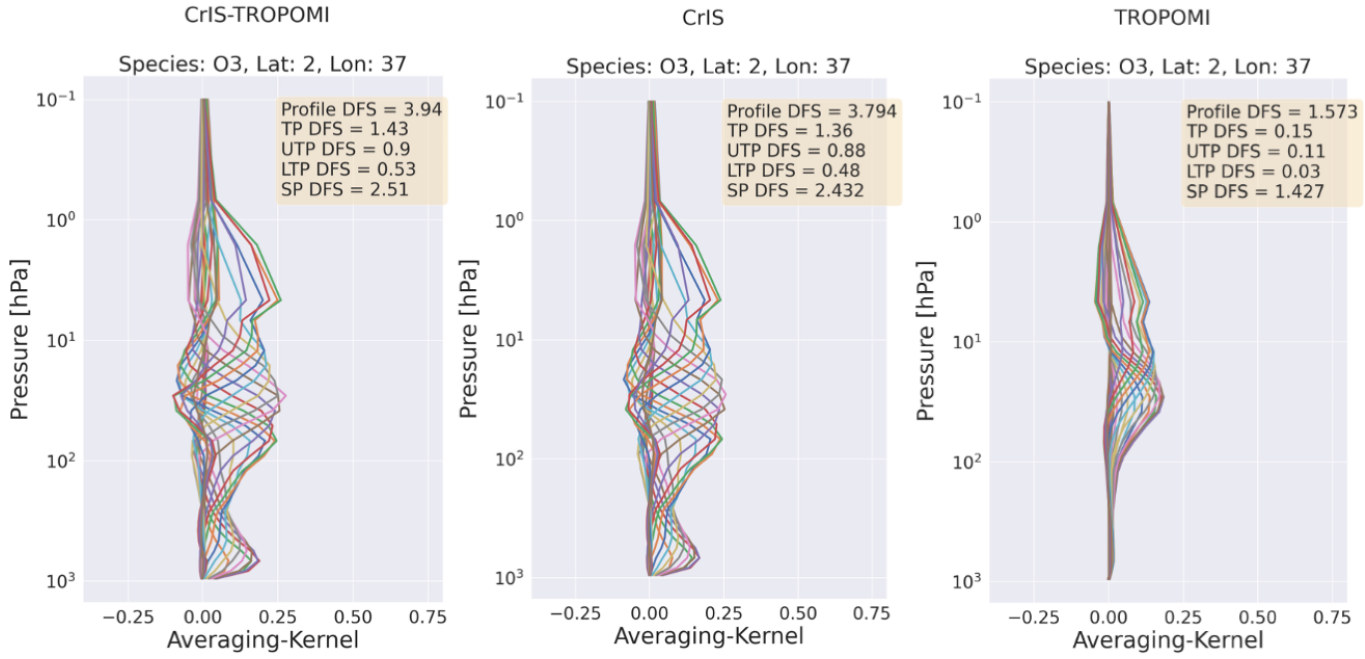

Figure 16. Example theoretical AKs comparisons for CrIS-TROPOMI/CrIS/TROPOMI using the 314-340 nm window in the TROPOMI UVIS band. DFS values for the total profile as well as separate sub-columns are indicated in each plot for comparison purposes.

7 Conclusions

MUSES TROPESS ozone profile retrievals from joint spectral measurements of Suomi NPP CrIS and S5P/TROPOMI are an important new product in understanding ozone variability. In the stratosphere we find improved performance over and above each instrument individually, based on an analysis of a month of intercomparisons. Cross comparisons of CrIS-TROPOMI/CrIS/TROPOMI,

with independent datasets from MLS, MUSES AIRS-OMI, show ~~in general~~ some positive results for CrIS-TROPOMI~~has the highest quality performance relative to the other instruments. Focusing~~ , especially focusing on stratospheric column comparisons with MLS the stratospheric 'gold standard' on August 12th 2020, a linear slope of 1.029, bias of -0.32 DU and correlation coefficient of 0.952 are found, highlighting the quality of the retrievals. A month long comparison in August 2020 shows a constantly lower bias between MLS and CrIS-TROPOMI and either CrIS or TROPOMI alone. Despite being a TIR instrument CrIS shows high linear correlation with MLS, indicating the utility of CrIS by itself. CrIS-only shows a linear slope of 0.921, bias of 3.8 DU and a correlation coefficient of 0.926. TROPOMI shows a significant bias, with a slope of 0.898. However, room for improvement is also identified, with large biases in the upper stratosphere identified with CrIS-TROPOMI.

The analysis of CrIS-only is highlighted, with CrIS capable of tropospheric estimates of ozone, with DFS values exceeding 2 in the tropics, roughly equally partitioned between the lower and upper troposphere. As with the CrIS-TROPOMI results, this is proven through comparisons with ozonesondes. CrIS-only shows a mean bias of between 1.4% and 10.4% depending on the season, comparable to that of AIRS-OMI (Fu et al., 2018). The performance in the troposphere for the joint retrieval is comparable to that of CrIS-only, with evidence that the joint retrieval provides benefit over CrIS-only with mean biases between 0.19% and 7.38%. CrIS-TROPOMI is in better agreement with ozonesondes at 316, 464 and 681 hPa in all seasons, except for a handful of cases (Table 8).

One of the key benefits of the joint retrieval is the use of single pixel retrievals, allowing for estimation of cloud properties, and the ability to see through clouds. Resulting in substantially larger data volumes in the final retrieval products.

~~Within the cross-comparison subsection, significant deviations are apparent between the MUSES retrievals, and the reanalysis datasets CAMS and MOMO-Chem. For example, CAMS finds relatively low tropospheric ozone concentrations in south east Asia (~20 DU), while MOMO-Chem identifies a significant enhancement (~100 DU). The causes of these differences should be investigated further. It is logical to assume that these differences occur with other reanalysis datasets. All MUSES retrievals, including this work, provide observational operators which can allow for the retrievals to be assimilated into these reanalysis datasets, for further improvement.~~

~~The MUSES~~ The MUSES CrIS-TROPOMI ozone retrieval is current not utilising its full potential; limited to using a short window within UVIS of TROPOMI. Pending the availability of soft-calibration calculations for TROPOMI windows, or improved L1b spectra (Ludewig et al., 2020; Mettig et al., 2021, 2022; Zhao et al., 2021). The MUSES algorithm is capable of processing daily TROPOMI and CrIS L1b spectra in near real time, and is flexible such that when better quality spectra become available, MUSES quickly be able to take advantage of any improvements. In preparation, we have shown the potential of CrIS-TROPOMI retrievals when using UV1 & UV2 of TROPOMI (Fig. 15), as well as a wider UVIS window (Fig. 16). The utilisation of UV1 and UV2 of TROPOMI provides a significant boost to the stratospheric DFS values ($\sim \times 2$), and can provide a moderate improvement to tropospheric DFS values ($\sim$0.5 DFS) for the example shown in this work.

The MUSES CrIS-TROPOMI ozone data set is a valuable new product for characterising the variation of ozone in the atmosphere. Future developments and refinements to the MUSES algorithm, will improve the product, and prepare MUSES for future applicable satellite instruments such as Sentinel 4, and joint retrievals from sentinel 5 and IASI-NG.

Both TROPOMI and CrIS are sensitive to trace gases other than ozone, for example carbon monoxide (Fu et al., 2016) and methane (bands 7 & 8 for TROPOMI). Therefore joint CrIS-TROPOMI retrievals offer an opportunity to explore potential improvements to other trace gas retrievals.

Code and data availability. MUSES data is available from https://tes.jpl.nasa.gov/tropess/get-data/products/. MLS data are available from https://daac.gsfc.nasa.gov/. TROPOMI L1b data, cloud products and CrIS L1b data are available from https://daac.gsfc.nasa.gov/. TROPOMI ILSF is available from http://www.tropomi.eu/data-products/isrf-dataset.

Appendix A: Impact of loss of CrIS Midwave Channels

As identified in sect. 2.1, from May 2021 CrIS lost the use of Mid-Wave due to instrument failure. Prior to this failure the MUSES CrIS retrieval algorithm made use of a number of windows in this band (Table 3). In this appendix we identify the possible impact of the loss of Mid-Wave on CrIS-TROPOMI/CrIS ozone retrievals by calculating the AKs of CrIS retrievals without the Mid-Wave windows. An example of these retrievals is identified in Fig. A1.

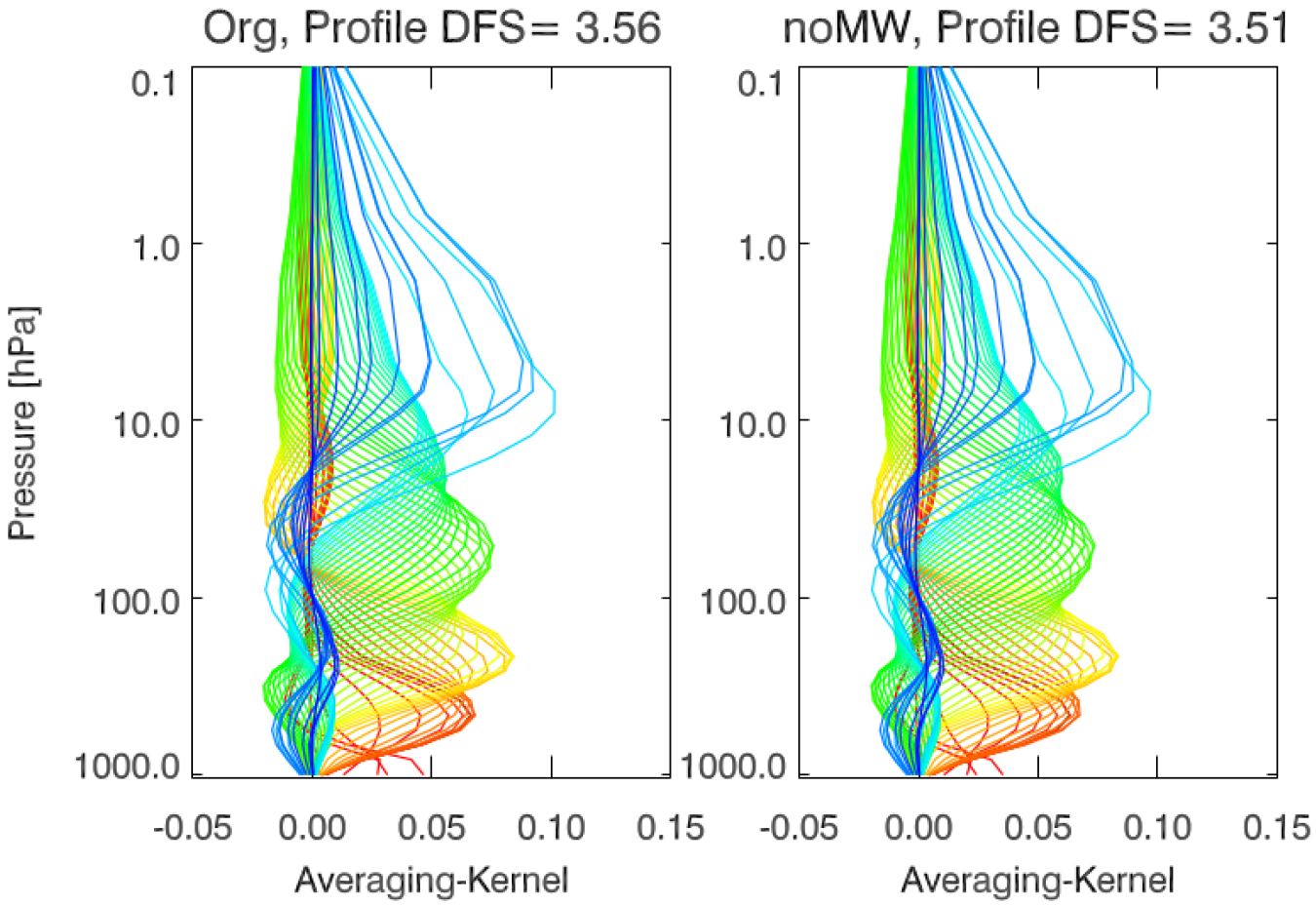

Figure A1. AKs from CrIS, the left hand plot shows an example with all of the original windows, the right hand plot indicates an example missing the Mid-Wave windows. The profile DFS values are identified in the title of each plot.

Figure A1 identifies only a minor loss of information content due to the loss of CrIS Mid-Wave, in this case a drop of 0.05 DFS. This suggests that the CrIS retrievals presented in this paper will only suffer a minor impact due to the loss of the Mid-Wave.

Appendix B: ~~Additional Cross-comparisons~~

~~Cross-comparisons of CAMS-reanalysis with CrIS, TROPOMI and CrIS-TROPOMI on August 12 2020 for the stratospheric profile. The structure of this figure is as Fig. 9.~~

~~Cross-comparisons of MUSES AIRS-OMI with CrIS, TROPOMI and CrIS-TROPOMI on August 12 2020 for the stratospheric profile. The structure of the figure is as shown in Fig. ??.~~

Appendix B: Further DFS Analysis

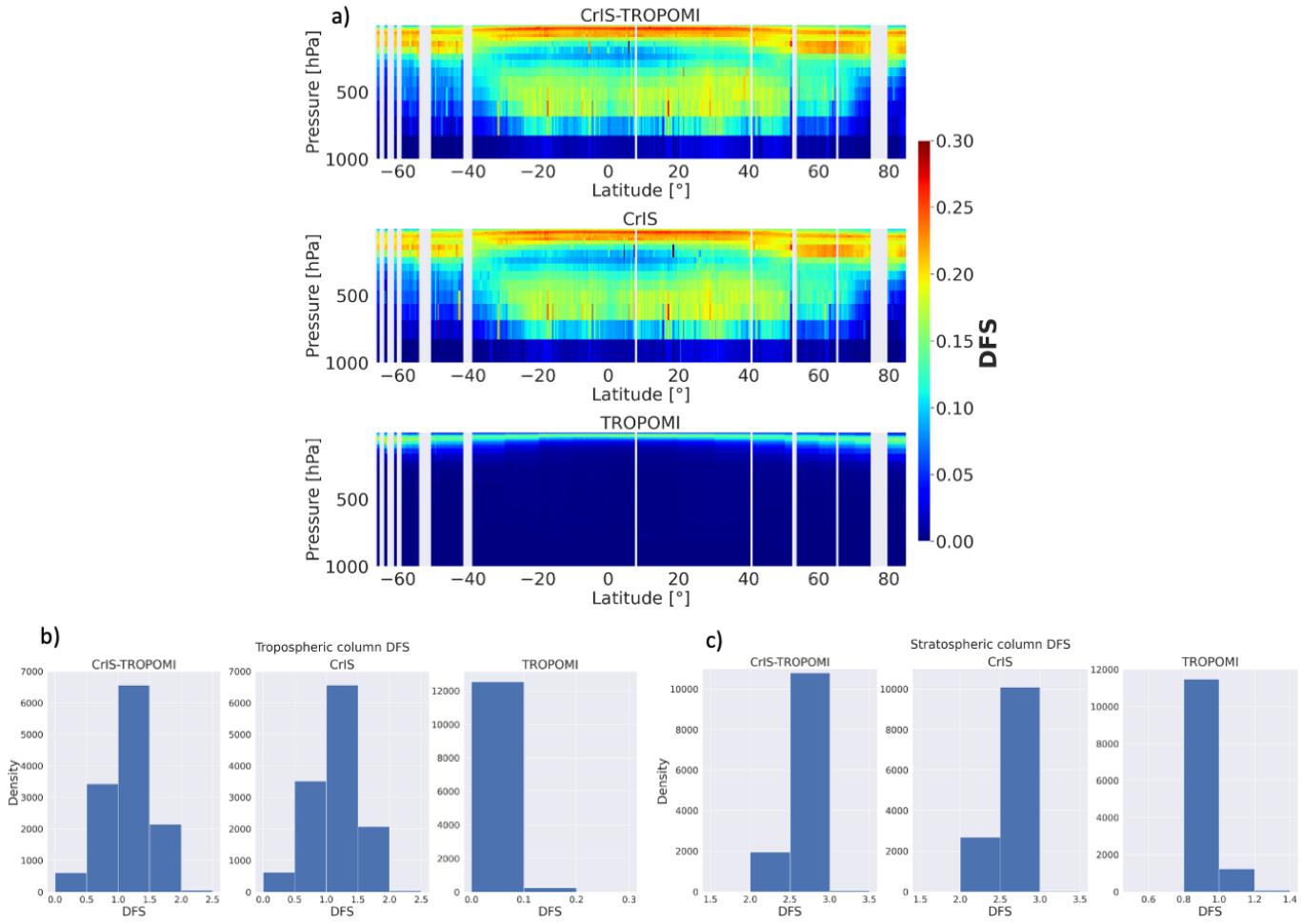

Figure B1. Visualisation of DFS values for August 12th 2020. Panel a) shows the distribution of DFS values over atmospheric layers for CrIS-TROPOMI/CrIS/TROPOMI. B) shows the spread of DFS values in the troposphere for the instruments, while c) shows the spread in the stratosphere.

Appendix C: Retrieved Ozone Profile Distribution

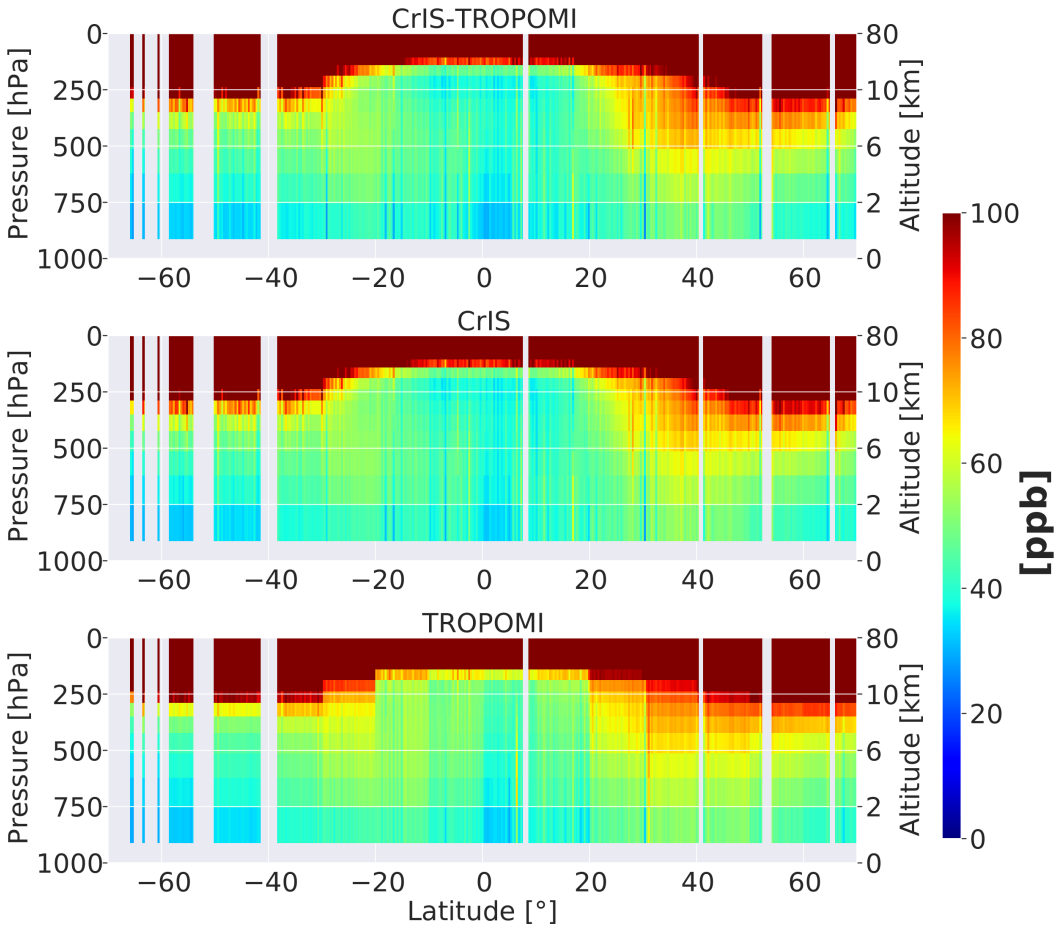

Figure C1. Vertical distribution of ozone binned into latitudinal bins, based on the data shown in Fig. 7. The titles of each subplot indicate the instrument.

Author contributions. EM implemented the CrIS-TROPOMI retrieval in MUSES, generated and analysed the data, and wrote the paper. VK developed the major components of MUSES, FO helped advanced MUSES, LK provided the data for AIRS-OMI comparisons and the analysis of the loss of CrIS Mid-Wave, GBO provided the ozonesonde comparison analysis, MDT implemented the ILSF of TROPOMI in MUSES. KWB, TPK, KM and VN guided, provided expertise and managed the research. All authors reviewed the paper.

Competing interests. The authors declare no competing interests.

Acknowledgements. A portion of this work was carried out at the Jet Propulsion Laboratory, California Institute of Technology, under a contract with the National Aeronautics and Space Administration (80NM0018D0004).

References

Aumann, H. H., Chahine, M. T., Gautier, C., Goldberg, M. D., Kalnay, E., McMillin, L. M., Revercomb, H., Rosenkranz, P. W., Smith, W. L., Staelin, D. H., Strow, L. L., and Susskind, J.: AIRS/AMSU/HSB on the aqua mission: Design, science objectives, data products, and processing systems, IEEE Transactions on Geoscience and Remote Sensing, 41, 253–263, https://doi.org/10.1109/TGRS.2002.808356, 2003.

Bloom, H. J.: The cross-track infrared sounder (CrIS): A sensor for operational meteorological remote sensing, in: International Geoscience and Remote Sensing Symposium (IGARSS), vol. 3, pp. 1341–1343, https://doi.org/10.1109/igarss.2001.976838, 2001.

Bowman, K. W., Steck, T., Worden, H. M., Worden, J., Clough, S., and Rodgers, C.: Capturing time and vertical variability of tropospheric ozone: A study using TES nadir retrievals, Journal of Geophysical Research: Atmospheres, 107, ACH 21–1–ACH 21–11, https://doi.org/10.1029/2002JD002150, 2002.

Bowman, K. W., Rodgers, C. D., Kulawik, S. S., Worden, J., Sarkissian, E., Osterman, G., Steck, T., Lou, M., Eldering, A., Shephard, M., Worden, H., Lampel, M., Clough, S., Brown, P., Rinsland, C., Gunson, M., and Beer, R.: Tropospheric Emission Spectrometer: Retrieval method and error analysis, IEEE Transactions on Geoscience and Remote Sensing, 44, 1297–1306, https://doi.org/10.1109/TGRS.2006.871234, 2006.

Bowman, K. W., Shindell, D. T., Worden, H. M., Lamarque, J. F., Young, P. J., Stevenson, D. S., Qu, Z., Torre, M. D. L., Bergmann, D., Cameron-Smith, P. J., Collins, W. J., Doherty, R., Dalsøren, S. B., Faluvegi, G., Folberth, G., Horowitz, L. W., Josse, B. M., Lee, Y. H., MacKenzie, I. A., Myhre, G., Nagashima, T., Naik, V., Plummer, D. A., Rumbold, S. T., Skeie, R. B., Strode, S. A., Sudo, K., Szopa, S., Voulgarakis, A., Zeng, G., Kulawik, S. S., Aghedo, A. M., and Worden, J. R.: Evaluation of ACCMIP outgoing longwave radiation from tropospheric ozone using TES satellite observations, Atmospheric Chemistry and Physics, 13, 4057–4072, https://doi.org/10.5194/ACP-13-4057-2013, 2013.

Brasseur, G. P., Hauglustaine, D. A., Walters, S., Rasch, P. J., Müller, J.-F., Granier, C., and Tie, X. X.: MOZART, a global chemical transport model for ozone and related chemical tracers: 1. Model description, Journal of Geophysical Research: Atmospheres, 103, 28 265–28 289, https://doi.org/10.1029/98JD02397, 1998.

Byrne, B., Liu, J., Lee, M., Yin, Y., Bowman, K. W., Miyazaki, K., Norton, A. J., Joiner, J., Pollard, D. F., Griffith, D. W. T., Velazco, V. A., Deutscher, N. M., Jones, N. B., and Paton-Walsh, C.: The Carbon Cycle of Southeast Australia During 2019–2020: Drought, Fires, and Subsequent Recovery, AGU Advances, 2, e2021AV000 469, https://doi.org/10.1029/2021AV000469, 2021.

Cai, Z., Liu, Y., Liu, X., Chance, K., Nowlan, C. R., Lang, R., Munro, R., and Suleiman, R.: Characterization and correction of Global Ozone Monitoring Experiment 2 ultraviolet measurements and application to ozone profile retrievals, Journal of Geophysical Research: Atmospheres, 117, n/a–n/a, https://doi.org/10.1029/2011JD017096, 2012.

Chance, K., Burrows, J., Perner, D., and Schneider, W.: Satellite measurements of atmospheric ozone profiles, including tropospheric ozone, from ultraviolet/visible measurements in the nadir geometry: a potential method to retrieve tropospheric ozone, Journal of Quantitative Spectroscopy and Radiative Transfer, 57, 467–476, https://doi.org/10.1016/S0022-4073(96)00157-4, 1997.

Clerbaux, C., Turquety, S., and Coheur, P.: Infrared remote sensing of atmospheric composition and air quality: Towards operational applications, Comptes Rendus Geoscience, 342, 349–356, https://doi.org/10.1016/j.crte.2009.09.010, 2010.

Colombi, N., Miyazaki, K., Bowman, K. W., Neu, J. L., and Jacob, D. J.: A new methodology for inferring surface ozone from multispectral satellite measurements, Environmental Research Letters, 16, 105 005, https://doi.org/10.1088/1748-9326/ac243d, 2021.

Crevoisier, C., Clerbaux, C., Guidard, V., Phulpin, T., Armante, R., Barret, B., Camy-Peyret, C., Chaboureau, J. P., Coheur, P. F., Crépeau, L., Dufour, G., Labonnote, L., Lavanant, L., Hadji-Lazaro, J., Herbin, H., Jacquinet-Husson, N., Payan, S., Péquignot, E., Pierangelo, C., Sellitto, P., and Stubenrauch, C.: Towards IASI-New Generation (IASI-NG): Impact of improved spectral resolution and radiometric noise on the retrieval of thermodynamic, chemistry and climate variables, Atmospheric Measurement Techniques, 7, 4367–4385, https://doi.org/10.5194/AMT-7-4367-2014, 2014.

Cuesta, J., Eremenko, M., Liu, X., Dufour, G., Cai, Z., Höpfner, M., von Clarmann, T., Sellitto, P., Foret, G., Gaubert, B., Beekmann, M., Orphal, J., Chance, K., Spurr, R., and Flaud, J.-M.: Satellite observation of lowermost tropospheric ozone by multispectral synergism of IASI thermal infrared and GOME-2 ultraviolet measurements over Europe, Atmospheric Chemistry and Physics, 13, 9675–9693, https://doi.org/10.5194/acp-13-9675-2013, 2013.

Cuesta, J., Kanaya, Y., Takigawa, M., Dufour, G., Eremenko, M., Foret, G., Miyazaki, K., and Beekmann, M.: Transboundary ozone pollution across East Asia: daily evolution and photochemical production analysed by IASI+GOME2 multispectral satellite observations and models, Atmospheric Chemistry and Physics, 18, 9499–9525, https://doi.org/10.5194/acp-18-9499-2018, 2018.

Danielson, J. and Gesch, D.: Global Multi-resolution Terrain Elevation Data 2010, Tech. rep., U.S. Geological Survey, https://doi.org/10.3133/OFR20111073, 2011.

Deeter, M. N., Martínez-Alonso, S., Edwards, D. P., Emmons, L. K., Gille, J. C., Worden, H. M., Sweeney, C., Pittman, J. V., Daube, B. C., and Wofsy, S. C.: The MOPITT Version 6 product: algorithm enhancements and validation, Atmos. Meas. Tech, 7, 3623–3632, https://doi.org/10.5194/amt-7-3623-2014, 2014.

Eichmann, K.-U., Kaiser, J., von Savigny, C., Rozanov, A., Rozanov, V., Bovensmann, H., von König, M., and Burrows, J.: SCIAMACHY limb measurements in the UV/Vis spectral region: first results, Advances in Space Research, 34, 775–779, https://doi.org/10.1016/j.asr.2003.05.057, 2004.

Eldering, A., Kulawik, S. S., Worden, J., Bowman, K., Osterman, G., Kulawik, S. S., Worden, J., Bowman, K., and Osterman, G.: Implementation of cloud retrievals for TES atmospheric retrievals: 2. Characterization of cloud top pressure and effective optical depth retrievals, Journal of Geophysical Research: Atmospheres, 113, 16–37, https://doi.org/10.1029/2007JD008858, 2008.

Emmons, L. K., Walters, S., Hess, P. G., Lamarque, J.-F., Pfister, G. G., Fillmore, D., Granier, C., Guenther, A., Kinnison, D., Laepple, T., Orlando, J., Tie, X., Tyndall, G., Wiedinmyer, C., Baughcum, S. L., and Kloster, S.: Description and evaluation of the Model for Ozone and Related chemical Tracers, version 4 (MOZART-4), Geoscientific Model Development, 3, 43–67, https://doi.org/10.5194/gmd-3-43-2010, 2010.

Fischer, H., Birk, M., Blom, C., Carli, B., Carlotti, M., Clarmann, T. V., Delbouille, L., Dudhia, A., Ehhalt, D., Endemann, M., Flaud, J. M., Gessner, R., Kleinert, A., Koopman, R., Langen, J., López-Puertas, M., Mosner, P., Nett, H., Oelhaf, H., Perron, G., Remedios, J., Ridolfi, M., Stiller, G., and Zander, R.: MIPAS: An instrument for atmospheric and climate research, Atmospheric Chemistry and Physics, 8, 2151–2188, https://doi.org/10.5194/ACP-8-2151-2008, 2008.

Flemming, J., Benedetti, A., Inness, A., J, R. E., Jones, L., Huijnen, V., Remy, S., Parrington, M., Suttie, M., Bozzo, A., Peuch, V. H., Akritidis, D., and Katragkou, E.: The CAMS interim Reanalysis of Carbon Monoxide, Ozone and Aerosol for 2003-2015, Atmospheric Chemistry and Physics, 17, 1945–1983, https://doi.org/10.5194/ACP-17-1945-2017, 2017.

Flynn, L., Long, C., Wu, X., Evans, R., Beck, C. T., Petropavlovskikh, I., McConville, G., Yu, W., Zhang, Z., Niu, J., Beach, E., Hao, Y., Pan, C., Sen, B., Novicki, M., Zhou, S., and Seftor, C.: Performance of the ozone mapping and profiler suite (OMPS) products, Journal of Geophysical Research, 119, 6181–6195, https://doi.org/10.1002/2013JD020467, 2014.

Froidevaux, L., Jiang, Y. B., Lambert, A., Livesey, N. J., Read, W. G., Waters, J. W., Browell, E. V., Hair, J. W., Avery, M. A., McGee, T. J., Twigg, L. W., Sumnicht, G. K., Jucks, K. W., Margitan, J. J., Sen, B., Stachnik, R. A., Toon, G. C., Bernath, P. F., Boone, C. D., Walker, K. A., Filipiak, M. J., Harwood, R. S., Fuller, R. A., Manney, G. L., Schwartz, M. J., Daffer, W. H., Drouin, B. J., Cofield, R. E., Cuddy, D. T., Jarnot, R. F., Knosp, B. W., Perun, V. S., Snyder, W. V., Stek, P. C., Thurstans, R. P., and Wagner, P. A.: Validation of Aura Microwave Limb Sounder stratospheric ozone measurements, Journal of Geophysical Research, 113, 15–20, https://doi.org/10.1029/2007jd008771, 2008.

Fu, D., Worden, J. R., Liu, X., Kulawik, S. S., Bowman, K. W., and Natraj, V.: Characterization of ozone profiles derived from Aura TES and OMI radiances, Atmospheric Chemistry and Physics, 13, 3445–3462, https://doi.org/10.5194/acp-13-3445-2013, 2013.

Fu, D., Bowman, K. W., Worden, H. M., Natraj, V., Worden, J. R., Yu, S., Veefkind, P., Aben, I., Landgraf, J., Strow, L., and Han, Y.: High-resolution tropospheric carbon monoxide profiles retrieved from CrIS and TROPOMI, Atmospheric Measurement Techniques, 9, 2567–2579, https://doi.org/10.5194/amt-9-2567-2016, 2016.

Fu, D., Kulawik, S. S., Miyazaki, K., Bowman, K. W., Worden, J. R., Eldering, A., Livesey, N. J., Teixeira, J., Irion, F. W., Herman, R. L., Osterman, G. B., Liu, X., Levelt, P. F., Thompson, A. M., and Luo, M.: Retrievals of tropospheric ozone profiles from the synergism of AIRS and OMI: Methodology and validation, Atmospheric Measurement Techniques, 11, 5587–5605, https://doi.org/10.5194/amt-11-5587-2018, 2018.

Garane, K., Lerot, C., Coldewey-Egbers, M., Verhoelst, T., Koukouli, M. E., Zyrichidou, I., Balis, D. S., Danckaert, T., Goutail, F., Granville, J., Hubert, D., Keppens, A., Lambert, J. C., Loyola, D., Pommereau, J. P., Roozendael, M. V., and Zehner, C.: Quality assessment of the Ozone-cci Climate Research Data Package (release 2017)-Part 1: Ground-based validation of total ozone column data products, Atmospheric Measurement Techniques, 11, 1385–1402, https://doi.org/10.5194/AMT-11-1385-2018, 2018.

Garane, K., Koukouli, M. E., Verhoelst, T., Lerot, C., Heue, K. P., Fioletov, V., Balis, D., Bais, A., Bazureau, A., Dehn, A., Goutail, F., Granville, J., Griffin, D., Hubert, D., Keppens, A., Lambert, J. C., Loyola, D., McLinden, C., Pazmino, A., Pommereau, J. P., Redondas, A., Romahn, F., Valks, P., Van Roozendael, M., Xu, J., Zehner, C., Zerefos, C., and Zimmer, W.: TROPOMI/S5P total ozone column data: Global ground-based validation and consistency with other satellite missions, Atmospheric Measurement Techniques, 12, 5263–5287, https://doi.org/10.5194/AMT-12-5263-2019, 2019.

Gettelman, A., Kinnison, D. E., Dunkerton, T. J., and Brasseur, G. P.: Impact of monsoon circulations on the upper troposphere and lower stratosphere, Journal of Geophysical Research: Atmospheres, 109, 1–14, https://doi.org/10.1029/2004JD004878, 2004.

Han, Y., Revercomb, H., Cromp, M., Gu, D., Johnson, D., Mooney, D., Scott, D., Strow, L., Bingham, G., Borg, L., Chen, Y., DeSlover, D., Esplin, M., Hagan, D., Jin, X., Knuteson, R., Motteler, H., Predina, J., Suwinski, L., Taylor, J., Tobin, D., Tremblay, D., Wang, C., Wang, L., Wang, L., and Zavyalov, V.: Suomi NPP CrIS measurements, sensor data record algorithm, calibration and validation activities, and record data quality, Journal of Geophysical Research: Atmospheres, 118, 12,734–12,748, https://doi.org/10.1002/2013JD020344, 2013.

Hitchman, M. H. and Rogal, M. J.: Influence of tropical convection on the Southern Hemisphere ozone maximum during the winter to spring transition, Journal of Geophysical Research: Atmospheres, 115, 14 118, https://doi.org/10.1029/2009JD012883, 2010.

Ingmann, P., Veihelmann, B., Langen, J., Lamarre, D., Stark, H., and Courrèges-Lacoste, G. B.: Requirements for the GMES Atmosphere Service and ESA's implementation concept: Sentinels-4/-5 and -5p, Remote Sensing of Environment, 120, 58–69, https://doi.org/10.1016/j.rse.2012.01.023, 2012.

IPCC: Climate Change 2013: The Physical Science Basis. Contribution of Working Group I to the Fifth Assessment Report of the Intergovernmental Panel on Climate Change, Cambridge University Press, http://www.ipcc.ch/report/ar5/wg2/, 2013.

Iturbide-Sanchez, F., Strow, L., Tobin, D., Chen, Y., Tremblay, D., Knuteson, R. O., Johnson, D. G., Buttles, C., Suwinski, L., Thomas, B. P., Rivera, A. R., Lynch, E., Zhang, K., Wang, Z., Porter, W. D., Jin, X., Predina, J. P., Eresmaa, R. I., Collard, A., Ruston, B., Jung, J. A., Barnet, C. D., Beierle, P. J., Yan, B., Mooney, D., and Revercomb, H.: Recalibration and Assessment of the SNPP CrIS Instrument: A Successful History of Restoration After Midwave Infrared Band Anomaly, IEEE Transactions on Geoscience and Remote Sensing, https://doi.org/10.1109/TGRS.2021.3112400, 2021.

Jaffe, D. A. and Wigder, N. L.: Ozone production from wildfires: A critical review, Atmospheric Environment, 51, 1–10, https://doi.org/10.1016/j.atmosenv.2011.11.063, 2012.

Jones, D. B. A., Bowman, K. W., Palmer, P. I., Worden, J. R., Jacob, D. J., Hoffman, R. N., Bey, I., Yantosca, R. M., Jones, C. ., Bowman, K. W., Palmer, P. I., Worden, J. R., Jacob, D. J., Hoffman, R. N., Bey, I., and Yantosca, R. M.: Potential of observations from the Tropospheric Emission Spectrometer to constrain continental sources of carbon monoxide, Journal of Geophysical Research: Atmospheres, 108, 4789, https://doi.org/10.1029/2003JD003702, 2003.

Kalnay, E., Kanamitsu, M., Kistler, R., Collins, W., Deaven, D., Gandin, L., Iredell, M., Saha, S., White, G., Woollen, J., Zhu, Y., Chelliah, M., Ebisuzaki, W., Higgins, W., Janowiak, J., Mo, K. C., Ropelewski, C., Wang, J., Leetmaa, A., Reynolds, R., Jenne, R., and Joseph, D.: The NCEP/NCAR 40-year reanalysis project, Bulletin of the American Meteorological Society, 77, 437–471, https://doi.org/10.1175/1520-0477(1996)077<0437:TNYRP>2.0.CO;2, 1996.

Kleipool, Q. L., Dobber, M. R., de Haan, J. F., and Levelt, P. F.: Earth surface reflectance climatology from 3 years of OMI data, Journal of Geophysical Research: Atmospheres, 113, 18 308, https://doi.org/10.1029/2008JD010290, 2008.

Komhyr, W. D., Barnes, R. A., Brothers, G. B., Lathrop, J. A., and Opperman, D. P.: Electrochemical concentration cell ozonesonde performance evaluation during STOIC 1989, Journal of Geophysical Research, 100, 9231–9244, https://doi.org/10.1029/94JD02175, 1995.

Kroon, M., de Haan, J. F., Veefkind, J. P., Froidevaux, L., Wang, R., Kivi, R., and Hakkarainen, J. J.: Validation of operational ozone profiles from the Ozone Monitoring Instrument, Journal of Geophysical Research, 116, D18 305, https://doi.org/10.1029/2010JD015100, 2011.

Kulawik, S. S., Worden, J., Eldering, A., Bowman, K., Gunson, M., Osterman, G. B., Zhang, L., Clough, S. A., Shephard, M. W., and Beer, R.: Implementation of cloud retrievals for Tropospheric Emission Spectrometer (TES) atmospheric retrievals: part 1. Description and characterization of errors on trace gas retrievals, Journal of Geophysical Research, 111, D24 204, https://doi.org/10.1029/2005JD006733, 2006.

Kulawik, S. S., Worden, J. R., Payne, V. H., Fu, D., Wofsy, S. C., McKain, K., Sweeney, C., Daube, B. C., Lipton, A., Polonsky, I., He, Y., Cady-Pereira, K. E., Dlugokencky, E. J., Jacob, D. J., and Yin, Y.: Evaluation of single-footprint AIRS CH4profile retrieval uncertainties using aircraft profile measurements, Atmospheric Measurement Techniques, 14, 335–354, https://doi.org/10.5194/amt-14-335-2021, 2021.

Landgraf, J. and Hasekamp, O. P.: Retrieval of tropospheric ozone: The synergistic use of thermal infrared emission and ultraviolet reflectivity measurements from space, Journal of Geophysical Research: Atmospheres, 112, 8310, https://doi.org/10.1029/2006JD008097, 2007.

Levelt, P. F., Oord, G. H. J. V. D., Dobber, M. R., Mälkki, A., Visser, H., Vries, J. D., Stammes, P., Lundell, J. O. V., and Saari, H.: The ozone monitoring instrument, IEEE Transactions on Geoscience and Remote Sensing, 44, 1093–1100, https://doi.org/10.1109/TGRS.2006.872333, 2006.

Levelt, P. F., Joiner, J., Tamminen, J., Veefkind, J. P., Bhartia, P. K., Zweers, D. C., Duncan, B. N., Streets, D. G., Eskes, H., Der, R. A. V., McLinden, C., Fioletov, V., Carn, S., Laat, J. D., Deland, M., Marchenko, S., McPeters, R., Ziemke, J., Fu, D., Liu, X., Pickering, K., Apituley, A., Abad, G. G., Arola, A., Boersma, F., Miller, C. C., Chance, K., Graaf, M. D., Hakkarainen, J., Hassinen, S., Ialongo, I., Kleipool, Q., Krotkov, N., Li, C., Lamsal, L., Newman, P., Nowlan, C., Suleiman, R., Tilstra, L. G., Torres, O., Wang, H.,

and Wargan, K.: The Ozone Monitoring Instrument: Overview of 14 years in space, Atmospheric Chemistry and Physics, 18, 5699–5745, https://doi.org/10.5194/ACP-18-5699-2018, 2018.

Liu, J. J., Jones, D. B., Worden, J. R., Noone, D., Parrington, M., and Kar, J.: Analysis of the summertime buildup of tropospheric ozone abundances over the Middle East and North Africa as observed by the Tropospheric Emission Spectrometer instrument, Journal of Geophysical Research: Atmospheres, 114, https://doi.org/10.1029/2008JD010993, 2009.

Liu, X., Chance, K., Sioris, C. E., Kurosu, T. P., Spurr, R. J. D., Martin, R. V., Fu, T.-M., Logan, J. A., Jacob, D. J., Palmer, P. I., Newchurch, M. J., Megretskaia, I. A., and Chatfield, R. B.: First directly retrieved global distribution of tropospheric column ozone from GOME: Comparison with the GEOS-CHEM model, Journal of Geophysical Research, 111, D02 308, https://doi.org/10.1029/2005JD006564, 2006.

Livesey, N. J., Filipiak, M. J., Froidevaux, L., Read, W. G., Lambert, A., Santee, M. L., Jiang, J. H., Pumphrey, H. C., Waters, J. W., Cofield, R. E., Cuddy, D. T., Daffer, W. H., Drouin, B. J., Fuller, R. A., Jarnot, R. F., Jiang, Y. B., Knosp, B. W., Li, Q. B., Perun, V. S., Schwartz, M. J., Snyder, W. V., Stek, P. C., Thurstans, R. P., Wagner, P. A., Avery, M., Browell, E. V., Cammas, J.-P., Christensen, L. E., Diskin, G. S., Gao, R.-S., Jost, H.-J., Loewenstein, M., Lopez, J. D., Nedelec, P., Osterman, G. B., Sachse, G. W., and Webster, C. R.: Validation of Aura Microwave Limb Sounder O 3 and CO observations in the upper troposphere and lower stratosphere, Journal of Geophysical Research, 113, 15–17, https://doi.org/10.1029/2007jd008805, 2008.

Loyola, D. G., García, S. G., Lutz, R., Argyrouli, A., Romahn, F., Spurr, R. J., Pedergnana, M., Doicu, A., García, V. M., and Schüssler, O.: The operational cloud retrieval algorithms from TROPOMI on board Sentinel-5 Precursor, Atmospheric Measurement Techniques, 11, 409–427, https://doi.org/10.5194/amt-11-409-2018, 2018.

Ludewig, A., Kleipool, Q., Bartstra, R., Landzaat, R., Leloux, J., Loots, E., Meijering, P., Van Der Plas, E., Rozemeijer, N., Vonk, F., and Veefkind, P.: In-flight calibration results of the TROPOMI payload on board the Sentinel-5 Precursor satellite, Atmospheric Measurement Techniques, 13, 3561–3580, https://doi.org/10.5194/amt-13-3561-2020, 2020.

Luo, M., Read, W., Kulawik, S., Worden, J., Livesey, N., Bowman, K., and Herman, R.: Carbon monoxide (CO) vertical profiles derived from joined TES and MLS measurements, Journal of Geophysical Research: Atmospheres, 118, 10,601–10,613, https://doi.org/10.1002/JGRD.50800, 2013.

Mettig, N., Weber, M., Rozanov, A., Arosio, C., Burrows, J. P., Veefkind, P., Thompson, A. M., Querel, R., Leblanc, T., Godin-Beekmann, S., Kivi, R., and Tully, M. B.: Ozone profile retrieval from nadir TROPOMI measurements in the UV range, Atmospheric Measurement Techniques, 14, 6057–6082, https://doi.org/10.5194/AMT-14-6057-2021, 2021.

Mettig, N., Weber, M., Rozanov, A., Burrows, J. P., Veefkind, P., Thompson, A. M., Stauffer, R. M., Leblanc, T., Ancellet, G., Newchurch, M. J., Kuang, S., Kivi, R., Tully, M. B., Malderen, R. V., Piters, A., Kois, B., Stübi, R., and Skrivankova, P.: Combined UV and IR ozone profile retrieval from TROPOMI and CrIS measurements, Atmospheric Measurement Techniques, 15, 2955–2978, https://doi.org/10.5194/AMT-15-2955-2022, 2022.

Miyazaki, K., Bowman, K., Sekiya, T., Eskes, H., Boersma, F., Worden, H., Livesey, N., Payne, V. H., Sudo, K., Kanaya, Y., Takigawa, M., and Ogochi, K.: Updated tropospheric chemistry reanalysis and emission estimates, TCR-2, for 2005-2018, Earth System Science Data, 12, 2223–2259, https://doi.org/10.5194/ESSD-12-2223-2020, 2020a.

Miyazaki, K., Bowman, W. K., Yumimoto, K., Walker, T., and Sudo, K.: Evaluation of a multi-model, multi-constituent assimilation framework for tropospheric chemical reanalysis, Atmospheric Chemistry and Physics, 20, 931–967, https://doi.org/10.5194/ACP-20-931-2020, 2020b.

Miyazaki, K., Bowman, K., Sekiya, T., Takigawa, M., Neu, J. L., Sudo, K., Osterman, G., and Eskes, H.: Global tropospheric ozone responses to reduced NOx emissions linked to the COVID-19 worldwide lockdowns, Science Advances, 7, https://doi.org/10.1126/SCIADV.ABF7460/SUPPL_FILE/SCIADV.ABF7460_SM.PDF, 2021.

Moncet, J. L., Uymin, G., Lipton, A. E., and Snell, H. E.: Infrared radiance modeling by optimal spectral sampling, Journal of the Atmospheric Sciences, 65, 3917–3934, https://doi.org/10.1175/2008JAS2711.1, 2008.

Moncet, J. L., Uymin, G., Liang, P., and Lipton, A. E.: Fast and accurate radiative transfer in the thermal regime by simultaneous optimal spectral sampling over all channels, Journal of the Atmospheric Sciences, 72, 2622–2641, https://doi.org/10.1175/JAS-D-14-0190.1, 2015.

Moré, J. J.: The Levenberg-Marquardt algorithm: Implementation and theory, https://doi.org/10.1007/bfb0067700, 1978.

NASES: Thriving on Our Changing Planet: A Decadal Strategy for Earth Observation from Space, National Academies Press, Washington DC, https://doi.org/10.17226/24938, 2018.

Natraj, V., Liu, X., Kulawik, S., Chance, K., Chatfield, R., Edwards, D. P., Eldering, A., Francis, G., Kurosu, T., Pickering, K., Spurr, R., and Worden, H.: Multi-spectral sensitivity studies for the retrieval of tropospheric and lowermost tropospheric ozone from simulated clear-sky GEO-CAPE measurements, Atmospheric Environment, 45, 7151–7165, https://doi.org/10.1016/j.atmosenv.2011.09.014, 2011.

Nicks, D., Baker, B., Lasnik, J., Delker, T., Chance, K., Liu, X., Flittner, D., Kim, J., and Howell, J.: Hyperspectral remote sensing of air pollution from geosynchronous orbit with GEMS and TEMPO, in: Earth Observing Missions and Sensors: Development, Implementation, and Characterization V, edited by Xiong, X. and Kimura, T., vol. 10781, p. 30, SPIE, https://doi.org/10.1117/12.2324781, 2018.

NOAA: CrIS on SNPP switch to side 1 on July 12, 2021, https://www.ospo.noaa.gov/data/messages/2021/MSG188150401.html, 2021.

NOAA: Geostationary and Extended Orbits (GeoXO) NOAA SATELLITE AND INFORMATION SERVICE | GOES-R SERIES PROGRAM OFFICE FACT SHEET, https://www.nesdis.noaa.gov/GeoXO, 2022.

Park, M., Randel, W. J., Kinnison, D. E., Garcia, R. R., and Choi, W.: Seasonal variation of methane, water vapor, and nitrogen oxides near the tropopause: Satellite observations and model simulations, Journal of Geophysical Research: Atmospheres, 109, n/a–n/a, https://doi.org/10.1029/2003JD003706, 2004.

Revercomb, H. and Strow, L.: Suomi NPP CrIS Level 1B Full Spectral Resolution V2, https://doi.org/10.5067/9NPOTPIPLMAW, 2018.

Rodgers, C. D.: Inverse Methods for Atmospheric Sounding - Theory and Practice, vol. 2, World Scientific, https://doi.org/10.1142/9789812813718, 2000.

Rothman, L. S., Gordon, I. E., Babikov, Y., Barbe, A., Chris Benner, D., Bernath, P. F., Birk, M., Bizzocchi, L., Boudon, V., Brown, L. R., Campargue, A., Chance, K., Cohen, E. A., Coudert, L. H., Devi, V. M., Drouin, B. J., Fayt, A., Flaud, J. M., Gamache, R. R., Harrison, J. J., Hartmann, J. M., Hill, C., Hodges, J. T., Jacquemart, D., Jolly, A., Lamouroux, J., Le Roy, R. J., Li, G., Long, D. A., Lyulin, O. M., Mackie, C. J., Massie, S. T., Mikhailenko, S., Müller, H. S., Naumenko, O. V., Nikitin, A. V., Orphal, J., Perevalov, V., Perrin, A., Polovtseva, E. R., Richard, C., Smith, M. A., Starikova, E., Sung, K., Tashkun, S., Tennyson, J., Toon, G. C., Tyuterev, V. G., and Wagner, G.: The HITRAN2012 molecular spectroscopic database, Journal of Quantitative Spectroscopy and Radiative Transfer, 130, 4–50, https://doi.org/10.1016/j.jqsrt.2013.07.002, 2013.

Sandu, A. and Chai, T.: Chemical Data Assimilation—An Overview, Atmosphere 2011, Vol. 2, Pages 426-463, 2, 426–463, https://doi.org/10.3390/ATMOS2030426, 2011.

Seemann, S. W., Borbas, E. E., Knuteson, R. O., Stephenson, G. R., and Huang, H. L.: Development of a global infrared land surface emissivity database for application to clear sky sounding retrievals from multispectral satellite radiance measurements, Journal of Applied Meteorology and Climatology, 47, 108–123, https://doi.org/10.1175/2007JAMC1590.1, 2008.

Seftor, C. J., Jaross, G., Kowitt, M., Haken, M., Li, J., and Flynn, L. E.: Postlaunch performance of the Suomi National Polar-orbiting Partnership Ozone Mapping and Profiler Suite (OMPS) nadir sensors, Journal of Geophysical Research: Atmospheres, 119, 4413–4428, https://doi.org/10.1002/2013JD020472, 2014.

Serdyuchenko, A., Gorshelev, V., Weber, M., Chehade, W., and Burrows, J. P.: High spectral resolution ozone absorption cross-sections ndash; Part 2: Temperature dependence, Atmospheric Measurement Techniques, 7, 625–636, https://doi.org/10.5194/AMT-7-625-2014, 2014.

Sinha, P., Jaeglé, L., Hobbs, P. V., and Liang, Q.: Transport of biomass burning emissions from southern Africa, Journal of Geophysical Research: Atmospheres, 109, 20 204, https://doi.org/10.1029/2004JD005044, 2004.

Smith, N. and Barnet, C. D.: Uncertainty Characterization and Propagation in the Community Long-Term Infrared Microwave Combined Atmospheric Product System (CLIMCAPS), Remote Sensing, 11, 1227, https://doi.org/10.3390/rs11101227, 2019.

Smith, N. and Barnet, C. D.: CLIMCAPS observing capability for temperature, moisture, and trace gases from AIRS/AMSU and CrIS/ATMS, Atmospheric Measurement Techniques, 13, 4437–4459, https://doi.org/10.5194/amt-13-4437-2020, 2020.

Spurr, R., de Haan, J., van Oss, R., and Vasilkov, A.: Discrete-ordinate radiative transfer in a stratified medium with first-order rotational Raman scattering, Journal of Quantitative Spectroscopy and Radiative Transfer, 109, 404–425, https://doi.org/10.1016/j.jqsrt.2007.08.011, 2008.

Spurr, R. J.: VLIDORT: A linearized pseudo-spherical vector discrete ordinate radiative transfer code for forward model and retrieval studies in multilayer multiple scattering media, Journal of Quantitative Spectroscopy and Radiative Transfer, 102, 316–342, https://doi.org/10.1016/j.jqsrt.2006.05.005, 2006.

Stolarski, R. S., Bloomfield, P., McPeters, R. D., and Herman, J. R.: Total Ozone trends deduced from Nimbus 7 Toms data, Geophysical Research Letters, 18, 1015–1018, https://doi.org/10.1029/91GL01302, 1991.

Suarez, M. J., Rienecker, M. M., Suarez, M. J., Todling, R., Bacmeister, J., Takacs, L., Liu, H.-C., Gu, W., Sienkiewicz, M., Koster, R. D., Gelaro, R., Stajner, I., and Nielsen, J. E.: Technical Report Series on Global Modeling and Data Assimilation, Volume 27 The GEOS-5 Data Assimilation System— Documentation of Versions 5.0.1, 5.1.0, and 5.2.0 The NASA STI Program Offi ce . . . in Profi le, Tech. rep., http://www.sti.nasa.gov/STI-homepage.html, 2008.

Susskind, J., Barnet, C. D., and Blaisdell, J. M.: Retrieval of atmospheric and surface parameters from AIRS/AMSU/HSB data in the presence of clouds, IEEE Transactions on Geoscience and Remote Sensing, 41, 390–409, https://doi.org/10.1109/TGRS.2002.808236, 2003.

Szopa, S., Naik, V., Adhikary, B., Artaxo, P., Berntsen, T., Collins, W. D., Fuzzi, S., Gallardo, L., Scharr, A. K., Klimont, Z., Liao, H., Unger, N., and Zanis, P.: Short-Lived Climate Forcers., 2021.

Thompson, A. M., Witte, J. C., Sterling, C., Jordan, A., Johnson, B. J., Oltmans, S. J., Fujiwara, M., Vömel, H., Allaart, M., Piters, A., Coetzee, G. J. R., Posny, F., Corrales, E., Diaz, J. A., Félix, C., Komala, N., Lai, N., Nguyen, H. T. A., Maata, M., Mani, F., Zainal, Z., Ogino, S.-y., Paredes, F., Penha, T. L. B., da Silva, F. R., Sallons-Mitro, S., Selkirk, H. B., Schmidlin, F. J., Stübi, R., and Thiongo, K.: First Reprocessing of Southern Hemisphere Additional Ozonesondes (SHADOZ) Ozone Profiles (1998–2016): 2. Comparisons With Satellites and Ground-Based Instruments, Journal of Geophysical Research: Atmospheres, 122, 13,000–13,025, https://doi.org/10.1002/2017JD027406, 2017.

Tweedy, O. V., Limpasuvan, V., Orsolini, Y. J., Smith, A. K., Garcia, R. R., Kinnison, D., Randall, C. E., Kvissel, O. K., Stordal, F., Harvey, V. L., and Chandran, A.: Nighttime secondary ozone layer during major stratospheric sudden warmings in specified-dynamics WACCM, Journal of Geophysical Research: Atmospheres, 118, 8346–8358, https://doi.org/10.1002/JGRD.50651, 2013.

Veefkind, J. P., Aben, I., McMullan, K., Förster, H., de Vries, J., Otter, G., Claas, J., Eskes, H. J., de Haan, J. F., Kleipool, Q., van Weele, M., Hasekamp, O., Hoogeveen, R., Landgraf, J., Snel, R., Tol, P., Ingmann, P., Voors, R., Kruizinga, B., Vink, R., Visser, H., and Levelt, P. F.: TROPOMI on the ESA Sentinel-5 Precursor: A GMES mission for global observations of the atmospheric composition for climate, air quality and ozone layer applications, Remote Sensing of Environment, 120, 70–83, https://doi.org/10.1016/j.rse.2011.09.027, 2012.

Waters, J. W., Froidevaux, L., Harwood, R. S., Jarnot, R. F., Pickett, H. M., Read, W. G., Siegel, P. H., Cofield, R. E., Filipiak, M. J., Flower, D. A., Holden, J. R., Lau, G. K., Livesey, N. J., Manney, G. L., Pumphrey, H. C., Santee, M. L., Wu, D. L., Cuddy, D. T., Lay, R. R., Loo, M. S., Perun, V. S., Schwartz, M. J., Stek, P. C., Thurstans, R. P., Boyles, M. A., Chandra, K. M., Chavez, M. C., Chen, G. S., Chudasama, B. V., Dodge, R., Fuller, R. A., Girard, M. A., Jiang, J. H., Jiang, Y., Knosp, B. W., Labelle, R. C., Lam, J. C., Lee, K. A., Miller, D., Oswald, J. E., Patel, N. C., Pukala, D. M., Quintero, O., Scaff, D. M., Van Snyder, W., Tope, M. C., Wagner, P. A., and Walch, M. J.: The Earth Observing System Microwave Limb Sounder (EOS MLS) on the aura satellite, IEEE Transactions on Geoscience and Remote Sensing, 44, 1075–1092, https://doi.org/10.1109/TGRS.2006.873771, 2006.

WHO: Health Aspects of Air Pollution with Particulate Matter, Ozone and Nitrogen Dioxide Report on a WHO Working Group OZONE-adverse effects NITROGEN DIOXIDE-adverse effects AIR POLLUTANTS, ENVIRONMENTAL-adverse effects META-ANALYSIS AIR-standards GUIDELINES, Tech. Rep. January, http://www.euro.who.int/__data/assets/pdf_file/0005/112199/E79097.pdf, 2003.

Witte, J. C., Thompson, A. M., Smit, H. G. J., Fujiwara, M., Posny, F., Coetzee, G. J. R., Northam, E. T., Johnson, B. J., Sterling, C. W., Mohamad, M., Ogino, S.-Y., Jordan, A., and da Silva, F. R.: First reprocessing of Southern Hemisphere ADditional OZonesondes (SHADOZ) profile records (1998–2015): 1. Methodology and evaluation, Journal of Geophysical Research: Atmospheres, 122, 6611–6636, https://doi.org/10.1002/2016JD026403, 2017.

Witte, J. C., Thompson, A. M., Smit, H. G. J., Vömel, H., Posny, F., and Stübi, R.: First Reprocessing of Southern Hemisphere ADditional OZonesondes Profile Records: 3. Uncertainty in Ozone Profile and Total Column, Journal of Geophysical Research: Atmospheres, 123, 3243–3268, https://doi.org/10.1002/2017JD027791, 2018.

Worden, H. M., Logan, J. A., Worden, J. R., Beer, R., Bowman, K., Clough, S. A., Eldering, A., Fisher, B. M., Gunson, M. R., Herman, R. L., Kulawik, S. S., Lampel, M. C., Luo, M., Megretskaia, I. A., Osterman, G. B., and Shephard, M. W.: Comparisons of Tropospheric Emission Spectrometer (TES) ozone profiles to ozonesondes: Methods and initial results, Journal of Geophysical Research: Atmospheres, 112, 3309, https://doi.org/10.1029/2006JD007258, 2007a.

Worden, J., Liu, X., Bowman, K., Chance, K., Beer, R., Eldering, A., Gunson, M., and Worden, H.: Improved tropospheric ozone profile retrievals using OMI and TES radiances, Geophysical Research Letters, 34, L01 809, https://doi.org/10.1029/2006GL027806, 2007b.

Worden, J., Jones, D. B., Liu, J., Parrington, M., Bowman, K., Stajner, I., Beer, R., Jiang, J., Thouret, V., Kulawik, S., Li, J. L. F., Verma, S., and Worden, H.: Observed vertical distribution of tropospheric ozone during the Asian summertime monsoon, Journal of Geophysical Research: Atmospheres, 114, 13 304, https://doi.org/10.1029/2008JD010560, 2009.

Worden, J., Kulawik, S., Frankenberg, C., Payne, V., Bowman, K., Cady-Peirara, K., Wecht, K., Lee, J.-E., and Noone, D.: Profiles of CH4, HDO, H2O, and N2O with improved lower tropospheric vertical resolution from Aura TES radiances, Atmospheric Measurement Techniques, 5, 397–411, https://doi.org/10.5194/amt-5-397-2012, 2012.

Worden, J. R., Turner, A. J., Bloom, A., Kulawik, S. S., Liu, J., Lee, M., Weidner, R., Bowman, K., Frankenberg, C., Parker, R., and Payne, V. H.: Quantifying lower tropospheric methane concentrations using GOSAT near-IR and TES thermal IR measurements, Atmos. Meas. Tech, 8, 3433–3445, https://doi.org/10.5194/amt-8-3433-2015, 2015.

Worden, J. R., Kulawik, S. S., Fu, D., Payne, V. H., Lipton, A. E., Polonsky, I., He, Y., Cady-Pereira, K., Moncet, J. L., Herman, R. L., Irion, F. W., and Bowman, K. W.: Characterization and evaluation of AIRS-based estimates of the deuterium content of water vapor, Atmospheric Measurement Techniques, 12, 2331–2339, https://doi.org/10.5194/amt-12-2331-2019, 2019.

Xiong, X., Liu, X., Wu, W., Knowland, K. E., Yang, Q., Welsh, J., and Zhou, D. K.: Satellite observation of stratospheric intrusions and ozone transport using CrIS on SNPP, Atmospheric Environment, 273, 118 956, https://doi.org/10.1016/J.ATMOSENV.2022.118956, 2022.

Young, P. J., Archibald, A. T., Bowman, K. W., Lamarque, J.-F., Naik, V., Stevenson, D. S., Tilmes, S., Voulgarakis, A., Wild, O., Bergmann, D., Cameron-Smith, P., Cionni, I., Collins, W. J., Dalsøren, S. B., Doherty, R. M., Eyring, V., Faluvegi, G., Horowitz, L. W., Josse, B., Lee, Y. H., MacKenzie, I. A., Nagashima, T., Plummer, D. A., Righi, M., Rumbold, S. T., Skeie, R. B., Shindell, D. T., Strode, S. A., Sudo, K., Szopa, S., and Zeng, G.: Pre-industrial to end 21st century projections of tropospheric ozone from the Atmospheric Chemistry and Climate Model Intercomparison Project (ACCMIP), Atmospheric Chemistry and Physics, 13, 2063–2090, https://doi.org/10.5194/acp-13-2063-2013, 2013.

Zavyalov, V., Esplin, M., Scott, D., Esplin, B., Bingham, G., Hoffman, E., Lietzke, C., Predina, J., Frain, R., Suwinski, L., Han, Y., Major, C., Graham, B., and Phillips, L.: Noise performance of the CrIS instrument, Journal of Geophysical Research: Atmospheres, 118, 13,108–13,120, https://doi.org/10.1002/2013JD020457, 2013.

Zhao, F., Liu, C., Cai, Z., Liu, X., Bak, J., Kim, J., Hu, Q., Xia, C., Zhang, C., Sun, Y., Wang, W., and Liu, J.: Ozone profile retrievals from TROPOMI: Implication for the variation of tropospheric ozone during the outbreak of COVID-19 in China, Science of The Total Environment, 764, 142 886, https://doi.org/10.1016/j.scitotenv.2020.142886, 2021.

Zoogman, P., Liu, X., Suleiman, R. M., Pennington, W. F., Flittner, D. E., Al-Saadi, J. A., Hilton, B. B., Nicks, D. K., Newchurch, M. J., Carr, J. L., Janz, S. J., Andraschko, M. R., Arola, A., Baker, B. D., Canova, B. P., Chan Miller, C., Cohen, R. C., Davis, J. E., Dussault, M. E., Edwards, D. P., Fishman, J., Ghulam, A., González Abad, G., Grutter, M., Herman, J. R., Houck, J., Jacob, D. J., Joiner, J., Kerridge, B. J., Kim, J., Krotkov, N. A., Lamsal, L., Li, C., Lindfors, A., Martin, R. V., McElroy, C. T., McLinden, C., Natraj, V., Neil, D. O., Nowlan, C. R., OSullivan, E. J., Palmer, P. I., Pierce, R. B., Pippin, M. R., Saiz-Lopez, A., Spurr, R. J., Szykman, J. J., Torres, O., Veefkind, J. P., Veihelmann, B., Wang, H., Wang, J., and Chance, K.: Tropospheric emissions: Monitoring of pollution (TEMPO), https://doi.org/10.1016/j.jqsrt.2016.05.008, 2017.